The LuxO-OpaR quorum-sensing cascade differentially controls Vibriophage VP882 lysis-lysogeny decision making in liquid and on surfaces

Francis J. Santoriello[1] and Bonnie L. Bassler[1,2]*

[1]Department of Molecular Biology, Princeton University, Princeton, NJ 08544, USA.

[2]Howard Hughes Medical Institute, Chevy Chase, MD 20815, USA.

*Corresponding author

Author email addresses:

fs1185@princeton.edu

bbassler@princeton.edu

KEYWORDS: quorum sensing, surface sensing, bacteriophage, lysogeny, *Vibrio parahaemolyticus*

ABSTRACT

Quorum sensing (QS) is a process of cell-to-cell communication that bacteria use to synchronize collective behaviors. QS relies on the production, release, and group-wide detection of extracellular signaling molecules called autoinducers. *Vibrio*s use two QS systems: the LuxO-OpaR circuit and the VqmA-VqmR circuit. Both QS circuits control group behaviors including biofilm formation and surface motility. The *Vibrio parahaemolyticus* temperate phage φVP882 encodes a VqmA homolog (called VqmAφ). When VqmAφ is produced by φVP882 lysogens, it binds to the host-produced autoinducer called DPO and launches the φVP882 lytic cascade. This activity times induction of lysis with high host cell density and presumably promotes maximal phage transmission to new cells. Here, we explore whether, in addition to induction from lysogeny, QS controls the initial establishment of lysogeny by φVP882 in naïve host cells. Using mutagenesis, phage infection assays, and phenotypic analyses, we show that φVP882 connects its initial lysis-lysogeny decision to both host cell density and whether the host resides in liquid or on a surface. Host cells in the low-cell-density QS state primarily undergo lysogenic conversion. The QS regulator LuxO~P promotes φVP882 lysogenic conversion of low-cell-density planktonic host cells. By contrast, the ScrABC surface-sensing system regulates lysogenic conversion of low-cell-density surface-associated host cells. ScrABC controls the abundance of the second messenger molecule cyclic diguanylate, which in turn, modulates motility. The *scrABC* operon is only expressed when its QS repressor, OpaR, is absent. Thus, at low-cell-density-QS-dependent derepression of *scrABC* drives lysogenic conversion in surface-associated host cells. These results demonstrate that φVP882 integrates cues from multiple sensory pathways into its lifestyle decision making upon infection of a new host cell.

AUTHOR SUMMARY

Bacteria in nature often exist in surface-associated communities including sessile biofilms and highly motile swarms. Thus, bacteriophages can encounter their hosts in structured communities. Much bacteriophage research is performed in homogenous, planktonic cultures containing cells that neither display the gene expression patterns nor the behaviors that occur in surface communities. The *Vibrio parahaemolyticus* temperate phage φVP882, after lysogenizing its host, can monitor the vicinal cell density and time lytic induction with high host cell density. Here, we show that, upon infection of a new host cell, φVP882 assesses host cell density to make the decision whether to lyse or lysogenize. Host cells at low density primarily undergo lysogenic conversion, and the components driving the phage decision-making process vary depending on whether the host cell is in liquid or associated with a solid surface. We propose that by tuning its lysis-lysogeny decision making to both host cell density and the physical environment of the host, φVP882 can maximize transmission to new host cells and dispersal to new environments.

55 **INTRODUCTION**

56 Quorum-sensing (QS) communication between bacteria dictates whether cells undertake
57 individual or group behaviors. QS relies on the production, release, accumulation, and detection
58 of extracellular signaling molecules called autoinducers, and the process allows bacteria to
59 synchronize collective activities (1,2). The model QS bacterium and pathogen *Vibrio*
60 *parahaemolyticus* uses two QS systems. The first system is the LuxO-OpaR cascade (Fig. 1A),
61 in which three autoinducers (called AI-1, AI-2, and CAI-1) are detected by membrane-bound
62 receptors that modulate the phosphorylation state of LuxO to control production of non-coding
63 RNAs called the Qrr sRNAs (3–8). At low cell density, LuxO is phosphorylated (LuxO~P), the Qrr
64 sRNAs are produced, and they repress production of the high-cell-density master regulator OpaR.
65 Under this condition, *V. parahaemolyticus* cells act as individuals. At high cell density (the mode
66 depicted in Fig. 1A), autoinducer detection drives dephosphorylation of LuxO, the Qrr sRNAs are
67 not made, and OpaR is produced. OpaR controls a regulon of genes underpinning group
68 behaviors (9–11). The second QS system consists of the cytoplasmic autoinducer receptor and
69 transcription factor VqmA (Fig. 1A), which binds the autoinducer called DPO and drives the
70 production of a sRNA called VqmR. VqmR, in turn, controls genes required for group behaviors
71 (12,13).

72

73 When *V. parahaemolyticus* associates with a solid surface, it can embark on one of two QS-
74 controlled lifestyles: swarming motility at low cell density or biofilm formation at high cell density
75 (9,10). OpaR regulates these behaviors directly and indirectly, the latter through the ScrABC
76 sensory pathway (14–16; and Fig. 1B). The *scrABC* operon encodes the aminotransferase ScrA,
77 periplasmic binding protein ScrB, and diguanylate cyclase/phosphodiesterase ScrC. ScrA
78 produces a molecule known as the S-signal that binds ScrB (16,17). In the absence of S-signal,
79 ScrC functions as a diguanylate cyclase, increasing the intracellular pool of cyclic diguanylate (c-
80 di-GMP) to induce exopolysaccharide production and biofilm formation (15,18,19). ScrB bound to

81 the S-signal interacts with ScrC on the inner membrane, which triggers the ScrC
82 phosphodiesterase activity. Degradation of c-di-GMP reduces the c-di-GMP pool, which activates
83 production of lateral flagella and swarming motility (15,16). Other phosphodiesterases (ScrG and
84 TpdA) and diguanylate cyclases (ScrJ, ScrL, and GefA) also modulate these behaviors, with
85 ScrABC functioning as the primary controller of c-di-GMP abundance during growth on a surface
86 (20–24). Regarding the connection between QS and surface sensing, OpaR represses *scrABC*
87 and thus, suppresses swarming motility at high cell density (10; and Fig. 1B). This OpaR function
88 drives an increase in the c-di-GMP pool and a shift toward biofilm formation. During surface
89 growth, OpaR also represses the *lafK* gene encoding the transcriptional activator of the lateral
90 flagellar (*laf*) operon while OpaR activates the *cpsR* and *cpsQ* genes encoding transcriptional
91 activators of the exopolysaccharide (*cps*) operon (11,18,25–27). The net effect of these OpaR
92 functions is suppression of swarming and activation of biofilm formation at high cell density.
93
94 Phages in nature encounter and infect bacterial hosts that exist as individual planktonic cells or
95 in surface-attached biofilm communities (28,29). Following infection of a host cell, a temperate
96 phage either replicates and lyses the host or enters a dormant state of genome maintenance
97 called lysogeny (30–32). It is known that in model temperate phages such as phage λ, the
98 outcome of the lysis-lysogeny decision depends on the multiplicity of infection (MOI). Specifically,
99 the higher the MOI, the more lysogeny that occurs (33,34). In the lysogenic state, the phage
100 genome, or prophage, either integrates into the host genome (i.e., λ) or is maintained as an
101 extrachromosomal plasmid-like element (i.e., P1, N15) (32,35,36). Lysogens can activate and
102 become lytic. Traditionally, lytic induction was understood to occur exclusively in response to host
103 cell stress such as DNA damage (31,32,37,38). New research has upended this dogma by
104 revealing that phages can monitor host sensory cues and exploit the information they garner to
105 drive lysogeny-lysis transitions (39–43). The *V. parahaemolyticus* plasmid-like phage VP882
106 (called φVP882) “eavesdrops” on host QS communication via a phage-encoded homolog of

107 VqmA (called VqmAφ) that allows the phage to monitor the abundance of host DPO (39; and Fig.
108 1A). At high host cell density, VqmAφ binds to DPO and activates production of the phage anti-
109 repressor Qtip that sequesters the phage cI repressor and triggers production of the lytic regulator
110 Q, and Q promotes host cell lysis. Presumably, lysing the host exclusively at high cell density
111 allows the phage to maximize transmission to new hosts. VqmAφ-dependent induction of φVP882
112 from lysogeny is also regulated by the LuxO-OpaR QS pathway (43). Specifically, host *V.*
113 *parahaemolyticus* strains with functional QS systems express higher levels of the φVP882 lytic
114 genes than strains locked in the low-cell-density QS state. These results indicate that multiple QS
115 pathways can influence φVP882 lifestyle transitions.
116
117 While QS clearly drives φVP882 lytic induction, the initial φVP882 commitment to lysis or lysogeny
118 that occurs upon infection of a naïve host has not been studied. Here, we investigated whether
119 the *V. parahaemolyticus* LuxO-OpaR QS system plays a role in this initial φVP882 lysis-lysogeny
120 decision. Further, given the known connection between OpaR, surface sensing, and surface
121 group behaviors including swarming and biofilm formation, we explored whether the host's
122 physical environment influences the initial φVP882 lysis-lysogeny decision. Specifically, we
123 quantified lysogeny and phage virion production during φVP882 infection of wildtype (WT) *V.*
124 *parahaemolyticus* and a panel of *V. parahaemolyticus* QS mutants in both planktonic and surface-
125 associated contexts. Our results demonstrate that the initial φVP882 lysis-lysogeny decision is
126 regulated by the host LuxO-OpaR QS system. First, the phage shows an extreme preference for
127 establishing lysogeny in cells that exist in the low-cell-density QS state, both in liquid and on a
128 surface. Regarding low-cell-density planktonic host cells, lysogeny is driven by LuxO~P through
129 the Qrr sRNAs via an OpaR-independent mechanism. In low-cell-density surface-associated host
130 cells, however, lysogeny is driven by the absence of OpaR, which enables derepression of the
131 surface-sensing operon – *scrABC*. ScrABC production leads to a decrease in cytoplasmic c-di-

132 GMP which, in turn, promotes increased φVP882-driven lysogenic conversion. Importantly, these
133 patterns are not due to an inability of φVP882 to infect *V. parahaemolyticus* cells at high cell
134 density, as infection of such cells leads to robust phage particle production. Our findings
135 demonstrate that φVP882 can incorporate cues from three different *V. parahaemolyticus* sensory
136 pathways (VqmA-VqmR, LuxO-OpaR, and ScrABC), allowing it to align its lifestyle transitions with
137 host cell density and particular environmental conditions.
138

139 **RESULTS**

140 ***V. parahaemolyticus* QS mutants for investigation of φVP882 infection outcomes**

141 *V. parahaemolyticus* O3:K6 strain RIMD2210633 (from here forward called RIMD) encodes
142 functional versions of all known QS components. To assess what effects host QS and downstream
143 changes in c-di-GMP abundance have on φVP882 infection outcomes, we constructed mutants
144 that lock RIMD into the low-cell-density and high-cell-density QS states. The low-cell-density-
145 locked strains are *luxO*^{D61E}, Δ*opaR*, and the double *luxO*^{D61E} Δ*opaR* and *luxO*^{D61A} Δ*opaR* mutants.
146 The high-cell-density-locked strain is *luxO*^{D61A}. The logic is as follows (see Fig. 1A): LuxO~P exists
147 at low cell density and dephosphorylated LuxO exists at high cell density. LuxO^{D61E} is a LuxO
148 phosphomimetic and LuxO^{D61A} cannot be phosphorylated. Thus, the *luxO*^{D61E} strain is locked into
149 the low-cell-density QS mode because it constitutively produces the Qrr sRNAs, and the *luxO*^{D61A}
150 strain is locked into the high-cell-density QS mode because it lacks Qrr sRNA production. OpaR
151 drives the high-cell-density QS program, and thus, the Δ*opaR* strain is locked into the low-cell-
152 density state. Likewise, because OpaR functions downstream of LuxO and the Qrr sRNAs, the
153 *luxO*^{D61E} Δ*opaR* and *luxO*^{D61A} Δ*opaR* double mutant strains are also locked into the low-cell-
154 density QS mode. These two strains differ in that the *luxO*^{D61E} Δ*opaR* strain produces the Qrr
155 sRNAs and the *luxO*^{D61A} Δ*opaR* strain does not. This difference will become important below.
156 Each of the above mutants displayed the expected low-cell-density or high-cell-density pattern of
157 expression of the known OpaR-activated gene *luxC* (P_{luxC}) (Fig. S1A). Moreover, the mutants
158 demonstrated the expected biofilm and swarming motility phenotypes – swarming when locked in
159 low-cell-density mode and biofilm formation when locked in high-cell-density mode (Fig. S1B,C,
160 respectively). All mutations were constructed in RIMD lacking exopolysaccharide production
161 (Δ*cpsA*) and polar flagellar motility (Δ*pomA*) as both are known to inhibit infection by some phages
162 (44,45). Eliminating these components enabled us to investigate φVP882 infection and its lysis-
163 lysogeny transitions without interference from obvious physical impediments to infection.

164

165 **An assay to quantify post-infection levels of φVP882 lysis and lysogeny of RIMD strains**

166 To investigate the role of QS in the initial φVP882 lysis-lysogeny decision upon infection of a naïve
167 RIMD host, we developed assays to quantify post-infection levels of lytic replication and lysogenic
168 conversion. φVP882 lytic replication was determined using quantitative polymerase chain
169 reactions (qPCR) against the φVP882 gene *gp69* on DNase-treated, cell-free culture fluids
170 collected from infected populations. This method enabled quantitation of capsid bound viral
171 genomes at the beginning and end of the φVP882 infection period. We used the values to
172 determine the amount of lytic replication that occurred in a population. Regarding lysogenic
173 conversion, for reasons we do not understand, insertion of an antibiotic resistance cassette into
174 the φVP882 genome resulted in a strong defect in phage infectivity. Thus, simple enumeration of
175 antibiotic resistant colonies to quantify lysogenic conversion post infection was not possible. To
176 circumvent this issue, we leveraged the φVP882 major lytic regulator Q (Fig. 1A). RIMD strains
177 carrying an arabinose-inducible copy of *q* on a plasmid (P_{bad}-*q*) were infected with φVP882 in
178 medium supplemented with $CaCl_2$, a requirement for phage adsorption and subsequent viral
179 entry. After 24 h, the cells were collected, diluted into fresh medium lacking $CaCl_2$, and Q
180 production was induced. Cells that had been lysogenized by φVP882 lysed while uninfected cells
181 did not die (Fig. 2A). Removal of $CaCl_2$ prior to induction of *q* ensured no subsequent rounds of
182 infection occurred. Thus, counterintuitively, quantitation of lysis could be used to calculate the
183 percentage of lysogenic conversion (% lysogens) in a population (see Materials and Methods).

184

185 To validate this method, we generated a lysogenic conversion standard curve by combining
186 known amounts of naïve RIMD cells with a stable RIMD φVP882 lysogen at ratios from 0%
187 lysogens to 100% lysogens. Both strains carried P_{bad}-*q*. Almost no lysis was detected in the mixed
188 cultures when grown in the absence of *q*-induction (Fig. S2A), indicating that the background level
189 of lytic induction in our experiments is low. Following *q*-induction, a stepwise increase in cell death

190 occurred that was proportional to the initial ratio of lysogens:naïve cells in each mixed culture
191 (Fig. S2B). The cell death data were used to calculate the percentage of lysogens within each
192 population, and those values agreed with the known ratios of lysogens:naïve cells dispensed into
193 each mixture (Fig. S2E). To ensure that the method worked reliably for each QS mutant, we
194 performed the *q*-induction assay with a fully lysogenized population of each of our strains (Fig.
195 S2F). Absent *q*-induction, only low-level lysis could be detected in each mutant. By contrast, *q*-
196 induction led to near total lysis (corresponding to 93-98% lysogenic conversion) in all mutants,
197 verifying the *q*-induction assay is unaffected by strain genotype. Finally, we validated the *q*-
198 induction assay against a standard curve of populations containing known quantities of lysogenic
199 cells that we generated by qPCR amplification of a segment of the phage genome. Such qPCR
200 analysis represents an established method for quantifying lysogens (46; and Fig. S2G-I). In our
201 case, the linear φVP882 prophage genome contains a *cos* site that is not present when the
202 genome is in the capsid-packaged configuration (Fig. S2G,H). Thus, qPCR amplification of the
203 *cos* region distinguishes φVP882 lysogens from φVP882 phage particles. The qPCR results were
204 comparable to those produced by *q*-induction (slopes of 0.98 and 0.86, respectively) (Fig. S2E,I).
205 The qPCR results confirm that *q*-induction delivers an accurate method to calculate the level of
206 lysogenic conversion in a population and it greatly increases the throughput of our analyses.
207

208 **LuxO phosphorylation and high MOI are necessary for φVP882 lysogenic conversion of**
209 **planktonic RIMD host cells**

210 Using the above methods to quantify φVP882 lytic replication and lysogenic conversion, we
211 investigated whether the LuxO-OpaR QS system regulates φVP882 infection outcomes in
212 planktonic RIMD cells. We first explored whether φVP882 infection outcomes depend on MOI.
213 We infected WT, low-cell-density-locked *luxO*^{D61E} and Δ*opaR* strains, and the high-cell-density-
214 locked *luxO*^{D61A} strain with φVP882 at phage:host ratios from 1:100 to 1:100,000. Fig. 2B shows
215 that after 24 h of infection, the WT and Δ*opaR* strains underwent MOI-dependent lysogenic

216 conversion, with high lysogenic conversion at high MOIs (56% and 86%, respectively) that
217 progressively decreased as MOI decreased. The high-cell-density-locked *luxO*^{D61A} strain
218 underwent significantly lower lysogenic conversion at each MOI. The low-cell-density-locked
219 *luxO*^{D61E} strain, however, showed high levels (>94%) of lysogenic conversion independent of MOI.
220 We investigated whether the differences in lysogenic conversion among the strains could be
221 attributed to differences in φVP882 adsorption. While φVP882 adsorbs to each strain, stronger
222 adsorption occurs to the low-cell-density-locked mutants than to the WT and high-cell-density-
223 locked *luxO*^{D61A} strain (Fig. S3A). Adsorption differences cannot, however, explain the different
224 patterns of lysogenic conversion between the *luxO*^{D61E} and Δ*opaR* low-cell-density-locked strains,
225 as the *luxO*^{D61E} strain shows high lysogenic conversion even at low MOIs while the Δ*opaR* strain
226 does not. Together, these results indicate that lysogenic conversion is regulated by MOI and the
227 phosphorylation state of LuxO.
228
229 **The Qrr sRNAs drive φVP882 lysogenic conversion in planktonic RIMD host cells**
230 **independently of OpaR**
231 In the LuxO-OpaR QS cascade, the Qrr sRNAs lie downstream of LuxO and upstream of OpaR
232 (Fig. 1A). At low cell density, LuxO~P activates expression of the *qrr* genes, and the Qrr sRNAs
233 repress *opaR*. One possible explanation for our above result showing a difference in the level of
234 lysogenic conversion that occurs when LuxO is phosphorylated versus that when OpaR is absent
235 is that, at low cell density, the Qrr sRNAs control φVP882 lysogenic conversion through some
236 OpaR-independent mechanism. To test this notion, we infected our set of RIMD strains carrying
237 P_{bad}-*q* with φVP882 for 24 h and measured the ensuing levels of lysis and lysogeny (Fig. 2A).
238
239 Regarding lysogenic conversion, no lysogenic conversion occurred in RIMD WT, which grows to
240 high cell density during the experiment, or in the high-cell-density-locked *luxO*^{D61A} strain (Fig. 2C

241 and Fig. S1A). By contrast, 96% lysogenic conversion occurred in both the *luxO*^{D61E} and *luxO*^{D61E}
242 Δ*opaR* low-cell-density-locked strains (Fig. 2C). Infection of the low-cell-density-locked Δ*opaR*
243 and *luxO*^{D61A} Δ*opaR* strains, however, resulted in only 12% and 0% lysogenic conversion,
244 respectively (Fig. 2C). These results suggest that in planktonic RIMD cells, LuxO^{D61E}-driven
245 constitutive production of the Qrr sRNAs causes φVP882 to undertake the lysogenic lifestyle via
246 an OpaR-independent mechanism. Importantly, these lysogenic conversion results do not parallel
247 the adsorption results (Fig. S3A). Specifically, the low-cell-density-locked Δ*opaR* strain shows
248 maximal adsorption (>99% particles adsorbed) but only undergoes 12% lysogenic conversion,
249 while the *luxO*^{D61E} Δ*opaR* double mutant undergoes both maximal adsorption and complete
250 lysogenic conversion. The difference in lysogenic conversion between these two strains suggests
251 that a mechanism other than viral attachment drives the propensity for lysogenic conversion to
252 occur. Regarding lysis, each of our test strains showed a >2,900-fold increase in production of
253 phage particles after 24 h of infection, demonstrating that each RIMD strain can be infected and
254 can promote φVP882 lytic replication (Fig. S3C). Phage particle production across the test strains
255 mirrored the adsorption capabilities (Fig. S3A), indicating that lytic replication is proportional to
256 the total number of attached phage particles. Basal-level spontaneous lytic induction in the
257 *luxO*^{D61E} and *luxO*^{D61E} Δ*opaR* strains accounts for their abilities to produce high numbers of phage
258 particles while having a high propensity for lysogenic conversion (Fig. S3E).
259
260 The results from the MOI and epistasis experiments (Fig. 2B,C) suggest that, for φVP882-directed
261 lysogenic conversion of RIMD to occur, a sufficiently high MOI must exist concurrent with the high-
262 level presence of Qrr sRNAs in the host cell. During experiments with 24 h infection periods in
263 which repeated rounds of infection occur, the MOI of φVP882 changes over time from low to high
264 as successive rounds of lytic replication and phage particle production occur. To assess the effects
265 of the Qrr sRNAs at discrete φVP882 MOIs, we captured the frequency of lysogenic conversion

266 that occurs in a single round of φVP882 infection. To do this, we measured lysogenic conversion
267 of our panel of test strains over two hours both at low and at high MOIs. At the low MOI, lysogenic
268 conversion could not be detected in any strain, while at the high MOI, lysogenic conversion
269 occurred in all strains, albeit significantly more frequently in strains possessing high levels of Qrr
270 sRNAs (i.e., in the Δ*opaR* and *luxO*^{D61E} Δ*opaR* strains) than in the strain possessing only low
271 levels of the Qrr sRNAs (i.e., in the *luxO*^{D61A} Δ*opaR* strain) (Fig. 2D). Again, these data suggest
272 that lysogenic conversion is favored when multiple φVP882 particles infect a cell harboring high
273 levels of Qrr sRNAs.
274
275 We reasoned that under conditions where the required MOI is met, if the Qrr sRNAs are indeed
276 responsible for driving φVP882 lysogenic conversion of RIMD at low cell densities, then
277 overexpression of *qrr* genes should promote lysogeny at high cell density. To test this idea, we
278 introduced tetracycline-inducible *qrr*2 (P_{tet}-*qrr*2) on a vector into our test strains and examined its
279 effect on the ability of φVP882 to lysogenize. The Qrr sRNAs share high sequence identity, and
280 *qrr*2 is the most highly expressed of the five *qrr* genes in RIMD, which is why we selected it for
281 this analysis (Fig. S4A). Furthermore, Qrr2 alone is sufficient to repress *opaR* and drive low-cell-
282 density behaviors in RIMD (47). We validated Qrr2 production from our construct in *E. coli* by
283 demonstrating its ability to bind the *opaR* mRNA 5' UTR and repress translation and in RIMD by
284 showing its ability to repress luciferase production from an OpaR-activated P_{luxC} transcriptional
285 reporter (Fig. S4B,C, respectively). As expected, the *luxO*^{D61E} strain underwent near total
286 lysogenic conversion when it carried the empty vector (EV) or the P_{tet}-*qrr*2 construct when
287 uninduced (EV = 93% and P_{tet}-*qrr*2 = 97%) or induced with anhydrotetracycline (aTc) (EV = 93%
288 and P_{tet}-*qrr*2 = 98%) (Fig. 2E). Presumably, lysogenic conversion occurs in the uninduced cultures
289 because, at low cell density, there is high-level native production of Qrr sRNAs from the
290 chromosome, and that saturates the putative mRNA target controlling φVP882 lysogenic

291 conversion. In the WT and *luxO*^{D61A} strains, by contrast, minimal lysogenic conversion occurred
292 when they carried the *qrr*2 construct in the absence of induction (WT = 20% and *luxO*^{D61A} = 0%).
293 Induction of *qrr*2 significantly increased the level of lysogenic conversion in the WT and the
294 *luxO*^{D61A} strain (WT = 75% and *luxO*^{D61A} = 24%) (Fig. 2E). The difference between the results for
295 the WT and the *luxO*^{D61A} mutant are likely due to the WT strain producing endogenous Qrr sRNAs
296 during the low-cell-density growth phase compared to the lower endogenous Qrr sRNA production
297 that occurs in the high-cell-density-locked *luxO*^{D61A} mutant (Fig. S4A). These results support our
298 hypothesis that high-level production of Qrr sRNAs at low cell density drives φVP882 lysogenic
299 conversion of planktonic host cells following infection. Given that OpaR is dispensable for this
300 effect (Fig. 2B,C), to direct lysogenic conversion, the Qrr sRNAs must target a currently unknown
301 host or φVP882 mRNA transcript.
302
303 **Derepression of the *scrABC* operon encoding the surface sensing system at low cell**
304 **density is required for φVP882 lysogenic conversion of surface-associated RIMD cells**
305 The RIMD LuxO-OpaR QS cascade modulates surface behaviors including biofilm formation and
306 swarming motility (10). At low cell density, the ScrABC surface sensing system catalyzes
307 degradation of the c-di-GMP pool which promotes lateral flagella production and swarming motility
308 (14–16). At high cell density, OpaR directly represses the *scrABC* and lateral flagellar operons,
309 while directly activating the *cps* operon (11,18,25–27; and Fig. 1B). Thus, OpaR drives an
310 increase in the c-di-GMP pool, reduced lateral flagella production, and increased
311 exopolysaccharide production, all of which promote biofilm formation. With our new knowledge
312 that LuxO~P and high Qrr sRNA levels foster φVP882 lysogenic conversion during infection of
313 planktonic RIMD cells, we wondered whether components of the LuxO-OpaR QS cascade, which
314 are intimately connected to the regulation of surface behaviors, also control φVP882 lysogenic
315 conversion of RIMD when the cells are associated with a surface. For this analysis, we again
316 used qPCR to quantify lytic replication and our P_{bad}-*q* lysogeny assay to quantify lysogenic

317 conversion, but the analyses were performed following 24 h infection of RIMD strains grown on
318 filters that are impermeable to both bacteria and phage particles on 1.5% agar plates. Importantly,
319 we validated that the *q*-induction assay functions reliably for cells harvested from filters on agar
320 surfaces (Fig. S2C-F). Similar to planktonic cells, φVP882 adsorbs to all of the test strains, albeit
321 with less affinity to WT and *luxO*^{D61A} strains than to the low-cell-density-locked strains (Fig. S3B).
322
323 Levels of φVP882 lysogenic conversion of surface associated RIMD strains were generally lower
324 than those in infections carried out in liquid (Fig. 3A). Strikingly, however, the pattern of φVP882
325 lysogenic conversion across the surface associated RIMD strains was different from that in
326 planktonic cells. Analogous to what occurred in planktonic infections, only low-level lysogenic
327 conversion occurred in surface-associated WT and high-cell-density-locked *luxO*^{D61A} RIMD cells
328 following φVP882 infection (8% and <1%, respectively; Fig. 3A). However, unlike in infections
329 carried out in liquid, all the Δ*opaR* strains underwent significant lysogenic conversion when
330 infected on a surface (39%, 43%, and 31% for Δ*opaR*, *luxO*^{D61E} Δ*opaR*, and *luxO*^{D61A} Δ*opaR*,
331 respectively; Fig. 3A). The *luxO*^{D61E} strain, in which *opaR* is repressed by the Qrr sRNAs but not
332 absent, showed a lower but still significant increase in lysogenic conversion (24%) compared to
333 WT RIMD (Fig. 3A). Unlike what we showed for planktonic cells (Fig. 2C and Fig. S3A), lysogenic
334 conversion in surface-associated cells correlates with adsorption affinity (Fig. 3A and Fig. S3B),
335 indicating that attachment to the host cell may be a driving feature on a surface. As with the
336 planktonic strains, we verified that all strains could be infected by φVP882 and could produce new
337 viral particles by lytic replication (Fig. S3D,F). Higher overall viral particle production occurred in
338 surface-associated strains compared to what occurred during planktonic infections (Fig. S3D),
339 indicating a possible preference of φVP882 for lysis over lysogeny during infection on a surface
340 (Fig. 3A).
341

342 Collectively, the data indicate that, unlike during infection of RIMD in liquid where OpaR-
343 independent Qrr sRNA activity controls lysogenic conversion, OpaR regulates the establishment
344 of lysogeny on a surface. Specifically, on surfaces, the absence of OpaR leads to increased
345 φVP882 lysogenic conversion, and therefore, OpaR must repress φVP882 lysogenic conversion.
346 Indeed, complementation of the Δ*opaR* strain with tetracycline-inducible *opaR* (P_{tet}-*opaR*) led to
347 a complete loss of lysogenic conversion on the surface (Fig. 3B). We verified that *opaR* was
348 expressed using P_{luxC} and P_{cpsA} transcriptional reporters, both of which are activated by OpaR
349 (Fig. S5A,B, respectively). These results demonstrate that φVP882 lysogenic conversion is
350 controlled by distinct QS regulators depending on whether the host cells are infected during
351 planktonic or surface-associated growth.
352
353 A key difference between planktonic and surface-grown RIMD strains is that increased expression
354 of the *scrABC* operon encoding the ScrABC surface sensing system occurs during low-cell-
355 density surface growth (10,48; and Fig. S6A). The ScrABC system is activated by mechanical
356 cues upon surface association and is further modulated by cell density via OpaR regulation (Fig.
357 1B and Fig. S6A). These features make ScrABC a good candidate to confer context-dependent
358 regulation of φVP882 lysogenic conversion of RIMD. To investigate this notion, we deleted
359 *scrABC* from each of our test strains. As above, we infected the strains with φVP882 on filters on
360 agar surfaces. Deletion of the *scrABC* operon led to a large reduction in lysogenic conversion in
361 each test strain (Fig 3A), but it did not impair φVP882 adsorption to cells (Fig. S3B). This finding
362 indicates that, analogous to planktonic cell infection outcomes, aspects other than φVP882
363 attachment to the host mediate lysogenic conversion in surface-associated cells. These results
364 suggest that the de-repression of the *scrABC* operon that occurs in the absence of OpaR at low
365 cell density enables φVP882 to establish lysogeny during surface infection.
366

367 **Degradation of the global c-di-GMP pool leads to increased φVP882 lysogenic conversion**
368 **of RIMD**
369 The ScrABC surface sensing system controls surface behaviors through modulation of the
370 intracellular c-di-GMP pool. When *scrABC* is expressed in RIMD cells on a surface at low cell
371 density (Fig. S6A), ScrC behaves as a phosphodiesterase and degrades c-di-GMP (15). To verify
372 this activity, we used a fluorescent reporter (49) to assess c-di-GMP abundance across planktonic
373 and surface-associated RIMD strains. Irrespective of growth condition, all Δ*opaR* strains
374 possessed less c-di-GMP than when OpaR was present, and the reductions in c-di-GMP
375 abundance were more dramatic in surface-associated RIMD compared to planktonic cells (Fig.
376 S6B). Together, these results are consistent with activation of *scrABC* expression and
377 phosphodiesterase activity in Δ*opaR* strains following surface association.
378
379 We assessed whether *scrABC*-dependent degradation of the c-di-GMP pool is sufficient to trigger
380 φVP882 lysogenic conversion in RIMD. We ensured that we could produce decreases and
381 increases, respectively, in c-di-GMP abundance using tetracycline-inducible constructs to
382 overexpress *scrABC* (P_{tet}-*scrABC*) harboring the WT *scrC* in which ScrC functions as a
383 phosphodiesterase or a mutant ScrC (P_{tet}-$scrC^{E554A}$) that functions exclusively as a diguanylate
384 cyclase (15; and Fig. S6C). We verified that ScrABC and the mutant $ScrC^{E554A}$ were produced
385 using a transcriptional reporter for the lateral flagellin (P_{lafA}), which is highly expressed during
386 swarming due to ScrABC-driven decreases in c-di-GMP abundance and is repressed by
387 $ScrC^{E554A}$-driven increases in c-di-GMP (Fig. S6D,E, respectively). With this strategy in hand, we
388 once again infected the Δ*scrABC* and Δ*opaR* strains on agar surfaces (Fig. 4A). As a reminder,
389 on a surface, the Δ*scrABC* strain possesses high c-di-GMP and undergoes minimal lysogenic
390 conversion, while the Δ*opaR* strain possesses low c-di-GMP and undergoes high-level lysogenic
391 conversion (Fig. 3A). Thus, these two strains allow us to maximally follow increases (Δ*scrABC*)

392 and decreases (Δ*opaR*) in lysogenic conversion in response to alterations in c-di-GMP
393 abundance. Complementation of the Δ*scrABC* strain with P_{tet}-*scrABC* restored lysogenic
394 conversion to levels exceeding that in the Δ*opaR* strain (Fig. 4A; EV = 0% and P_{tet}-*scrABC* =
395 58%). By contrast, overexpression of $scrC^{E554A}$ resulted in near complete loss of lysogenic
396 conversion in the Δ*opaR* strain (Fig. 4A; EV = 30% and P_{tet}-$scrC^{E554A}$ = 2%). Together, these
397 results support QS- and ScrABC-dependent alterations to the c-di-GMP pool as key to driving
398 φVP882 lysogenic conversion of surface-associated RIMD cells. Importantly, lysogenic
399 conversion during planktonic infection was unaffected by deletion of *scrABC.* Specifically, in liquid,
400 both the $luxO^{D61E}$ and $luxO^{D61E}$ Δ*scrABC* mutants underwent near total lysogenic conversion (96%
401 and 97%, respectively; Fig. 4B). This result is consistent with our finding and previously reported
402 data showing that *scrABC* is repressed in planktonic culture (48; and Fig. S6A,B). Thus, c-di-
403 GMP-driven modulation of φVP882 lysogenic conversion is specific to surface-associated host
404 cells.
405
406 c-di-GMP binding effector proteins can respond to changes in the global c-di-GMP pool and/or to
407 changes in local c-di-GMP abundance driven by specific diguanylate cyclases and
408 phosphodiesterases (50,51). To test whether the c-di-GMP responsive factor(s) driving φVP882
409 lysogenic conversion of surface-associated RIMD strains respond to a global reduction in the c-
410 di-GMP pool or whether they respond specifically to changes driven by ScrC phosphodiesterase
411 activity, we performed our surface infection experiments following modulation of c-di-GMP levels
412 using the RIMD phosphodiesterase TpdA and the RIMD diguanylate cyclase GefA. We
413 constructed P_{tet}-*tpdA* and P_{tet}-*gefA* and verified their activities by measuring their effects on c-di-
414 GMP abundance and lateral flagellin expression. As expected, production of TpdA and GefA had
415 opposite effects; TpdA reduced the c-di-GMP pool and increased *lafA* expression, while GefA
416 increased the c-di-GMP pool and reduced *lafA* expression (Fig. S6F-H). Fig. 4C shows that

417 overexpression of *tpdA* in the Δ*scrABC* strain restored lysogenic conversion (EV = 21% and P_{tet}-
418 *tpdA* = 75%). By contrast, overexpression of *gefA* resulted in the loss of lysogenic conversion in
419 the Δ*opaR* strain (EV = 75% and P_{tet}-*gefA* = 22%). Thus, reductions in the global c-di-GMP pool,
420 that need not be exclusively catalyzed by the ScrC phosphodiesterase, promote lysogenic
421 conversion of RIMD on surfaces.
422
423

DISCUSSION

In this report, we identified *V. parahaemolyticus* sensory components that control the φVP882 lysis-lysogeny decision during infection of naïve host cells. We discovered that *V. parahaemolyticus* RIMD cells can be infected and lysed by φVP882 at all cell densities, but *V. parahaemolyticus* RIMD cells at low cell density favor lysogenic conversion. Key was our finding that the sensory components necessary to drive lysogenic conversion varied based on the physical environment of the infected host cell. Specifically, high-level Qrr sRNA production drives lysogenic conversion in low-cell-density planktonic host cells, while ScrABC-directed degradation of the global c-di-GMP pool drives lysogenic conversion in low-cell-density surface-associated host cells. The components and mechanisms connecting the Qrr sRNAs and ScrABC to φVP882 lysogenic conversion capability are currently unknown.

Our data support the following scenario: When φVP882 initially encounters a susceptible host cell, it can adsorb at any cell density, albeit with greater affinity to cells in the low-cell-density QS state. After genome entry, φVP882 must lyse or lysogenize its host. Lysis is considered the default outcome for temperate phages (31), which is consistent with our results, as infected RIMD strains at all cell densities produce viral particles proportional to the level of phage adsorption. In model temperate phages such as phage λ, the primary mechanism promoting lysogeny is a high MOI because when multiple phage genomes enter the infected cell, a high dose of lysogeny-promoting phage regulatory proteins is supplied (33,34). The discovery of phage-bacterial and phage-phage communication systems that measure extracellular small molecule signals that modulate phage lifestyle decision making, however, has added new regulatory complexity to the rather straightforward notion of MOI as the main arbiter of the lysis-lysogeny decision (39,42,43,52–54). Our results show that in the case of φVP882, the initial lysis-lysogeny decision is controlled by both MOI and the phosphorylation state of LuxO. When RIMD cells are infected at a high MOI

449 and at low density, i.e., when LuxO is phosphorylated, lysogenic conversion is preferred. During
450 planktonic growth, maximal production of the Qrr sRNAs drives lysogenic conversion through an
451 OpaR-independent mechanism (Fig. 5, top left). When associated with a surface, Qrr sRNA
452 repression of OpaR production leads to derepression of the *scrABC* operon and degradation of
453 the global c-di-GMP pool, which promote φVP882 lysogenic conversion (Fig. 5, bottom left). We
454 expect that this mechanism involves an unknown c-di-GMP responsive effector. The Qrr sRNAs
455 and ScrABC are both situated downstream of LuxO in the *V. parahaemolyticus* QS cascade (Fig.
456 1), suggesting that LuxO is the master regulator of the φVP882 lysis-lysogeny decision. This idea
457 is further bolstered when we consider data concerning φVP882 induction from lysogeny.
458 Lysogenic φVP882 undergoes lytic induction when its VqmAφ QS receptor/transcription factor
459 detects the autoinducer DPO at high host cell density (39). Dephosphorylation of LuxO at high
460 cell density leads to increased VqmAφ-dependent lytic induction (43; and Fig. 5, right). While not
461 investigated here, it is possible that LuxO-dependent regulation of lysogenic conversion and
462 VqmAφ-dependent regulation of lytic induction are connected. Specifically,
463 phosphorylation/dephosphorylation of LuxO may enable toggling between φVP882 lysogeny (via
464 Qrr sRNAs or ScrABC, depending on the physical context of the host) and lysis (via DPO-VqmAφ)
465 both when the initial lysis-lysogeny decision is made and later in infection when the decision to
466 transition from lysogeny maintenance to lytic induction is undertaken (Fig. 5). Alternatively, it is
467 possible that the connection between LuxO phosphorylation/dephosphorylation and φVP882
468 lysis-lysogeny transitions is indirect and due to φVP882 detection of a shift in general host
469 physiology that is triggered by the Qrr sRNAs in planktonic cells and decreased c-di-GMP in
470 surface-associated cells.
471
472 Concerning the role of c-di-GMP, our results indicate that the φVP882 lysis-lysogeny decision is
473 only affected by OpaR-dependent changes in the global c-di-GMP pool when RIMD cells are
474 infected on a surface, not when they are in liquid (Fig. 4A,B). Our results and other published

475 work, however, have demonstrated that OpaR promotes shifts in the global c-di-GMP pool in both
476 planktonic and surface-associated RIMD cells (24,55; and Fig. S6B). This apparent inconsistency
477 cannot simply be explained by ScrABC activation being restricted to surface growth because
478 TpdA, a phosphodiesterase that is highly active in planktonic cells (24), was also capable of
479 driving φVP882 lysogenic conversion of RIMD (Fig. 4C). This finding suggests that the specific c-
480 di-GMP responsive effector(s) that drives φVP882 lysogenic conversion might only be
481 produced/active in surface associated cells. The RIMD genome encodes many known and
482 putative c-di-GMP responsive effectors, of which three have been shown to control surface
483 phenotypes – ScrO, CpsS, and CpsQ (18,19,56), making them potential candidates for future
484 exploration of host factors involved in φVP882 lysogenic conversion on a surface. In an analogous
485 vein, high-level Qrr sRNA production was not sufficient to drive lysogenic conversion in surface-
486 associated cells in the absence of ScrABC (Fig. 3A). Following the same logic as above, perhaps
487 the Qrr sRNAs only drive lysogenic conversion in planktonic cells because their downstream
488 target is a planktonic-specific factor(s). Possessing surface growth- and planktonic growth-
489 specific intermediate factors could provide RIMD an effective mechanism to confine the influences
490 of the Qrr sRNAs and c-di-GMP abundance to their respective physical contexts despite both the
491 Qrr sRNAs and c-di-GMP having other roles in planktonic and surface-associated cells (22,24,47).
492
493 Previously, we hypothesized that φVP882 integrates host cell density information into its lysis-
494 lysogeny transitions to ensure lytic replication is favored under conditions that maximize
495 transmission to new host cells (39,43). The preference for lysogeny over lysis in host cells at low
496 cell density aligns with this maximum transmission hypothesis. Indeed, we show here that
497 lysogeny occurs in the presence of high Qrr sRNA levels and low c-di-GMP abundance, both of
498 which coincide with maximal phosphorylation of LuxO and the absence of OpaR, i.e., low-cell-
499 density conditions. Germane to the present work is that, at low cell density, when OpaR levels are
500 at their lowest, *V. parahaemolyticus* cells are more motile than at high cell density when OpaR is

501 present and is functioning to, respectively, directly and indirectly repress the polar (swimming)
502 and lateral flagellar systems (surface-associated swarming) (9,10,47,57,58). Perhaps
503 lysogenizing highly motile cells allows φVP882 to disperse its genome over greater distances
504 than could be achieved by virion particles released from lysed non-motile cells. Phage
505 "hitchhiking" has been demonstrated but is typically described as phage capsids non-specifically
506 binding to membrane components on non-host cells and being transported to locales in which
507 legitimate host cells reside, enabling phage infection and replication (59,60). The φVP882 low-
508 cell-density lysogeny mechanism we have uncovered here could be a form of "hitchhiking" that
509 allows φVP882 prophages to disseminate and exist in a dormant state until a high density of host
510 cells is achieved. Following dephosphorylation of LuxO and production of OpaR in such a high-
511 density population, motility is suppressed, VqmAφ is produced, and the switch to lytic induction
512 occurs.
513
514 Studies investigating connections between phage infection and QS have primarily focused on QS
515 regulation of host defenses against phage infection (61–69). QS control of phage lysis-lysogeny
516 transitions is a new area of study. As additional QS-responsive temperate phages are discovered
517 (39–42,70–72), probing lysis-lysogeny transition dynamics in the context of host QS-controlled
518 group behaviors could provide insight into the evolution of cross-domain phage-bacterial QS
519 interactions and the costs and benefits to each entity under particular environmental conditions.
520

521 **MATERIALS AND METHODS**

522 **Bacterial strains, reagents, and growth conditions**

523 *E. coli* strains were grown with aeration in Lysogeny Broth (LB-Miller, BD-Difco) at 37° C. *V.*
524 *parahaemolyticus* RIMD strains were grown with aeration in LB or LB with 2% NaCl at 30° C.
525 Strains used in the study are listed in Table S1. Unless otherwise noted, antibiotics, were used at:
526 100 µg mL^{-1} ampicillin (Amp, Sigma), 50 µg mL^{-1} kanamycin (Kan, GoldBio), 50 µg mL^{-1} polymyxin
527 B (Pb), 5 µg mL^{-1} chloramphenicol (Cm, Sigma), and 15 µg mL^{-1} gentamycin (Gm, Sigma). L-
528 arabinose (Sigma) and L-dextrose (Sigma) were supplied at a final concentration of 0.2%.
529 Anhydrotetracycline (aTc, Takara Bio) was supplied at a final concentration of 100 ng mL^{-1}.

530

531 **Cloning techniques**

532 All primers used for plasmid construction and qPCR, listed in Table S2, were obtained from
533 Integrated DNA Technologies. FastCloning was employed for plasmid assembly (73). Briefly, PCR
534 with iProof polymerase (Bio-Rad) was used to generate cloning inserts and linear plasmid
535 backbone DNA. In cases in which inserts could not be generated by PCR, fragments were
536 synthesized by Integrated DNA Technologies. In the case of pRE112, linear plasmid backbone
537 was generated by restriction digestion with SmaI (NEB). Plasmid backbone DNA was treated with
538 DpnI (NEB) to remove PCR template DNA. Cloning inserts and linear plasmid backbones were
539 added to chemically competent *E. coli* cells, and plasmid assembly was carried out by the
540 transformed cells. All assembled plasmids were verified by Sanger sequencing. Plasmids used in
541 this study are listed in Table S3. Transfer of plasmids into *V. parahaemolyticus* RIMD strains was
542 carried out by conjugation followed by selective plating on LB plates supplemented with
543 appropriate antibiotics. Point mutations and deletion mutants were generated by allelic exchange
544 with sucrose counterselection. Mutations were verified by colony PCR and Sanger sequencing.

545

546 **Phage purification, concentration, and titering**

547 An overnight culture of *V. parahaemolyticus* strain 882 (the original strain from which φVP882 was
548 first isolated) carrying φVP882 and arabinose-inducible *vqmAφ* (P_{bad}-*vqmAφ*) on a vector was
549 diluted 1:100 into fresh LB with 2% NaCl and grown with aeration at 30° C until the culture reached
550 mid-logarithmic growth (OD_{600} = 0.2-0.4). At this point, arabinose was added to induce φVP882
551 lytic replication. Lysis was tracked by OD_{600} until the culture completely cleared. Cellular debris
552 was removed from the lysate by centrifugation (3000 rpm, 15 min). The supernatant was collected
553 and treated with DNase (Roche) and RNase (Roche) at 5 µg mL^{-1}, each, for 1 h at room
554 temperature, followed by filtration through a 0.22 µm bottle top vacuum filter (Millipore). The filtrate
555 was treated with 3% v/v Tween 80 and 35% m/v ammonium sulfate and was subjected to
556 centrifugation (3000 xg, 10 min, 4° C). The pellicle was collected and resuspended in SM buffer
557 (100 mM NaCl, 8 mM $MgSO_4$•$7H_2O$, 50 mM Tris-Cl). Phage stocks were titered by qPCR. Briefly,
558 an aliquot of phage stock was treated with RQ1 DNase (Promega) to remove remaining free DNA,
559 leaving only encapsidated phage genomes. Phage capsids were lysed during the DNase heat
560 denaturation step, and φVP882 genomes were quantified by qPCR with primers against the *gp69*
561 gene. Full degradation of free host genomic DNA by the DNase treatment was verified with
562 primers against the host *ompW* gene. Copy number was determined by absolute quantitation
563 against a standard curve of plasmid DNA harboring the *gp69* gene. Viable phage particles were
564 quantified by plaque assay. *V. parahaemolyticus* RIMD host cells were suspended in molten LB
565 medium containing 0.3% top agar and 10 mM $CaCl_2$. Suspensions were overlayed onto plates
566 containing LB medium and 1.5% agar. Ten-fold serial dilutions of phage stock (10^0 to 10^{-7}) were
567 spotted on the solidified top agar overlay. Plates were incubated for 18 h at 30° C to allow plaque
568 formation. Plaques were counted to calculate plaque forming units (PFU mL^{-1}).
569
570 **Quantitation of φVP882 adsorption, lytic replication, and lysogenic conversion during**
571 **planktonic and surface-associated infections**

572 To test φVP882 adsorption, overnight cultures of *V. parahaemolyticus* RIMD strains carrying an
573 arabinose-inducible copy of the φVP882 lytic regulator *q* (P_{bad}-*q*) were diluted 1:100 in fresh LB
574 medium containing 10 mM $CaCl_2$ and Kan. For planktonic cell adsorption assays, diluted cultures
575 were grown with aeration at 30° C for 4 h. Approximately 10^8 φVP882 particles were added to 250
576 µL of each culture. Phage-treated cultures and cell-free, phage-only controls were incubated
577 without shaking at 30° C for 10 min. The samples were gently pelleted (10 min, 500 xg, 4° C) to
578 remove cells and adsorbed phage particles. For surface-associated cell adsorption assays, 25 µL
579 of each diluted culture was spotted onto a 0.025 µm mixed cellulose ester (MCE) filter disc
580 (Millipore) placed on a dry agar surface (LB with 1.5% agar and Kan), and the samples were
581 incubated at 30° C for 18 h. *E. coli* TOP10 cells were spotted onto MCE filter discs placed on a
582 dry agar surface without Kan as the unadsorbed control. Filters were collected and suspended in
583 500 µL of LB medium containing 10 mM $CaCl_2$ and approximately 10^6 φVP882 particles. These
584 samples were subjected to vortex to remove the cells from the filters and allow them to become
585 mixed with the phage particles. The cells thus treated were incubated at 30° C for 20 min. Samples
586 were gently pelleted (10 min, 500 xg, 4° C) to remove any cells and adsorbed phage particles.
587 For both the planktonic cell and surface-associated cell samples, cell-free culture fluids were
588 collected, filter-sterilized through 96-well 0.22 µm filter plates (Millipore), and qPCR was
589 performed against the φVP882 *gp69* gene as described above to quantify unadsorbed phage
590 particles.
591
592 For infection of planktonic cells, overnight cultures of *V. parahaemolyticus* RIMD strains carrying
593 P_{bad}-*q* were diluted 1:100 in fresh LB containing 10 mM $CaCl_2$ and Kan. These diluted cultures
594 were treated with either φVP882 (MOIs are indicated in figure legends) or an equivalent volume
595 of SM buffer. Cultures were grown with aeration at 30° C for 24 h. Cells were collected and diluted
596 1:100 in fresh LB with Kan but lacking $CaCl_2$, which prevents subsequent rounds of infection by
597 phage particles produced due to Q-driven lytic induction. For infection of surface-associated cells,

598 immediately following treatment exactly as described for planktonic cells, 25 µL of the cultures
599 were spotted onto 0.025 µm MCE filter discs (Millipore) on a dry agar surface (LB with 1.5% agar
600 and Kan). Plates were incubated at 30° C for 24 h. Filter disks were removed from the agar plates
601 with sterile tweezers and transferred into 1 mL LB with Kan followed by vortex for 15 sec to
602 dislodge cells from filters. The suspensions were diluted 1:100 in fresh LB with Kan, again lacking
603 $CaCl_2$. When needed to maintain plasmids and to induce gene expression, Cm and aTc were
604 added to liquid media (planktonic infections) or to agar plates (surface infections) from the start
605 of the infection period.
606
607 To quantify φVP882 viral particle production following both planktonic and surface-associated
608 infections, cell-free culture fluids (0.22 µm filter-sterilized) were collected at T=0 and T=24 h of
609 infection. For surface infections, cell-free culture fluids were obtained from the initial cell
610 suspensions prior to spotting on the MCE filters (T0) and the post-infection cell suspensions
611 generated by vortex of the samples collected from the filters (T24). As described above, culture
612 fluids were treated with DNase, and encapsidated phage genomes were quantified by qPCR
613 against the φVP882 *gp69* gene.
614
615 Lysogenic conversion was quantified by *q*-induction. In all cases, after 24 h of infection, collection,
616 and dilution, aliquots of cultures were transferred in duplicate to a 96-well plate. Plates were
617 incubated at 30° C in a BioTek Synergy Neo2 Multi-Mode plate reader. Every 5 min, the plate was
618 shaken orbitally, and OD_{600} was measured. When cultures reached mid-logarithmic growth, L-
619 arabinose (*q*-induction) or L-dextrose (*q*-repression) was added. Plates were returned to the plate
620 reader and OD_{600} was measured every 5 min for the next 12 h. The measured OD_{600} values were
621 used to quantify the percentage of lysogenic conversion (% lysogens) in each population. To
622 quantitate lysogenic conversion after short periods of infection (0-2 h), qPCR was performed
623 against the φVP882 *cos* site and the host *ompW* gene. The number of phage genomes (*cos* site)

624 and host genomes (*ompW*) were determined by absolute quantitation against appropriate
625 standard curves. Because the φVP882 prophage is a multi-copy element, all *cos* site counts from
626 infected samples were normalized to the *cos* site copy number per cell for a stable φVP882
627 lysogen grown under the same conditions as the infected strain under study.
628
629 **Calculation of lysogenic conversion from Q-driven cell lysis**
630 Treatment with phage or SM buffer during the infection period and subsequent addition of L-
631 arabinose or L-dextrose resulted in four experimental conditions: SM buffer/+dextrose,
632 phage/+dextrose, SM buffer/+arabinose, phage/+arabinose. The following analysis was
633 performed for the arabinose-treated (*q* induction) samples and the dextrose-treated (*q* repression)
634 samples. The level of lysogenic conversion (% lysogens) was calculated for the arabinose-treated
635 and dextrose-treated samples using their respective phage-treated and buffer-treated conditions
636 and the following equation:

637 $$\%L = \left(\frac{OD_P - (OD_V/E)}{OD_P}\right) * 100$$
638
639 Here, OD_P and OD_V are the optical densities of the phage-treated cultures at the peak (pre-lysis)
640 and valley (post-lysis) of the growth curve. The peak and valley of each growth curve were
641 determined by setting a boundary at 4 h for planktonic infections and at 5 h for surface-associated
642 infections. OD_P is the maximum OD_{600} value before the boundary time and OD_V is the minimum
643 OD_{600} value after the boundary time. OD_V is divided by an expansion factor calculated from the
644 SM buffer-treated culture. The expansion factor can be represented by the ratio of the OD_{600} of
645 the SM buffer-treated culture at the timepoints corresponding to the peak (N_{tP}) and valley (N_{tV}) of
646 the infected culture. The expansion factor adjusts the infected culture OD_V value to correct for
647 continued growth of the non-lysogenized cells in that culture. We assume that induction of *q* in
648 the infected culture leads to complete lysis of all lysogenized cells. As the lysogenized cells lyse,
649 the growth rate of the non-lysogenized cells in that culture likely increases due to decreased

650 culture cell density and increased nutrient availability. Thus, when growth of the phage-treated
651 culture is reduced compared to the SM buffer-treated culture upon *q*-induction due to death of
652 lysogenized cells in the former ($N_{tV} / N_{tP} > OD_V / OD_P$), the expansion factor is scaled by the ratio
653 of OD_V to N_{tV} or the fold-reduction in OD_{600} between the SM buffer-treated culture and the phage-
654 treated culture.

655
$$\%L = \begin{cases} \left(\dfrac{OD_P - \left(OD_V / \left(\left(\frac{N_{tV}}{N_{tP}} \right) \right) \right)}{OD_P} \right) * 100, & \text{for } N_{tV}/N_{tP} \leq OD_V/OD_P \\ \left(\dfrac{OD_P - \left(OD_V / \left(\left(\frac{N_{tV}}{N_{tP}} \right) + \left(\left(\frac{N_{tV}}{OD_V} \right) - 1 \right) \right) \right)}{OD_P} \right) * 100, & \text{otherwise} \end{cases}$$

656

657 N_{tP} and N_{tV} are calculated with a basic form of the logistic equation commonly used in ecology
658 and evolution:

659
$$N_t = \frac{K}{1 + \left(\frac{K - N_0}{N_0} \right) e^{-rt}}$$

660

661 Here, N_0 represents the population size at the beginning of the growth curve. *K* represents the
662 carrying capacity of the culture. The intrinsic growth rate of the population is given by *r*. Finally, *t*
663 represents time. These parameters are determined by fitting the above logistic equation to the
664 experimental growth curves of the SM buffer-treated cultures using the R package growthcurver
665 (v 0.3.1) (74).

666

667 **Reporter Assays**

668 Overnight cultures of *V. parahaemolyticus* RIMD strains carrying bioluminescent or fluorescent
669 reporter constructs were diluted 1:100 in fresh LB with appropriate antibiotics except for strains
670 carrying the P_{luxC}-*luxCDABE* construct, which were diluted 1:1000. Overnight cultures of *E. coli*
671 strains carrying fluorescent reporter constructs were diluted 1:100 in fresh M9-glycerol with

672 appropriate antibiotics. In the case of planktonic cell assays, diluted cultures were dispensed (200
673 μL) into 96 well plates (Corning Costar). For surface-associated cell assays, diluted cultures were
674 spotted (3 μL) on solidified 1.5% LB agar (100 μL) with appropriate antibiotics in 96 well plates.
675 The liquid and agar media were supplemented with aTc, arabinose, or dextrose where specified.
676 Optical density, fluorescence, and bioluminescence were measured with a BioTek Synergy Neo2
677 Multi-Mode plate reader. In the case of *luxCDABE*-based transcriptional reporters, relative light
678 units (RLU) were calculated by dividing bioluminescence by optical density (for planktonic cell
679 assays) or by dividing bioluminescence by constitutive mScarlet-I signal from the host
680 chromosome (for surface-associated cell assays). If an experiment required reporter expression
681 to be compared between planktonic and surface conditions, bioluminescence was normalized to
682 constitutive mScarlet-I signal under both conditions. In the case of fluorescence-based
683 translational reporters in *E. coli*, relative fluorescence units (RFU) were calculated by dividing
684 GFP signal by optical density. Regarding the fluorescence-based c-di-GMP biosensor in *V.*
685 *parahaemolyticus* RIMD strains, RFU were calculated by dividing the TurboRFP reporter signal
686 by the constitutive AmCyan signal. Both fluorescent reporters are encoded on the same vector
687 (49).

688 **REFERENCES**

689 1. Papenfort K, Bassler BL. Quorum sensing signal–response systems in Gram-negative
690 bacteria. Nat Rev Microbiol. 2016;14(9):576–88.

691 2. Duddy OP, Bassler BL. Quorum sensing across bacterial and viral domains. PLoS Pathog.
692 2021;17(1):e1009074.

693 3. Lenz DH, Mok KC, Lilley BN, Kulkarni RV, Wingreen NS, Bassler BL. The Small RNA
694 Chaperone Hfq and Multiple Small RNAs Control Quorum Sensing in *Vibrio harveyi* and
695 *Vibrio cholerae*. Cell. 2004;118(1):69–82.

696 4. Waters CM, Bassler BL. The *Vibrio harveyi* quorum-sensing system uses shared regulatory
697 components to discriminate between multiple autoinducers. Genes Dev. 2006;20(19):2754–
698 67.

699 5. Shao Y, Bassler BL. Quorum-sensing non-coding small RNAs use unique pairing regions to
700 differentially control mRNA targets. Mol Microbiol. 2012;83(3):599–611.

701 6. Shao Y, Feng L, Rutherford ST, Papenfort K, Bassler BL. Functional determinants of the
702 quorum-sensing non-coding RNAs and their roles in target regulation. EMBO J.
703 2013;32(15):2158–71.

704 7. Feng L, Rutherford ST, Papenfort K, Bagert JD, van Kessel JC, Tirrell DA, et al. A Qrr
705 Noncoding RNA Deploys Four Different Regulatory Mechanisms to Optimize Quorum-
706 Sensing Dynamics. Cell. 2015;160(1–2):228–40.

707 8. Rutherford ST, Valastyan JS, Taillefumier T, Wingreen NS, Bassler BL. Comprehensive
708 analysis reveals how single nucleotides contribute to noncoding RNA function in bacterial
709 quorum sensing. Proc Natl Acad Sci USA. 2015;112(44):E6038-47.

710 9. McCarter LL. OpaR, a Homolog of *Vibrio harveyi* LuxR, Controls Opacity of *Vibrio*
711 *parahaemolyticus*. J Bacteriol. 1998;180(12):3166–73.

712 10. Gode-Potratz CJ, McCarter LL. Quorum Sensing and Silencing in *Vibrio parahaemolyticus*.
713 J Bacteriol. 2011;193(16):4224–37.

714 11. Kernell Burke A, Guthrie LTC, Modise T, Cormier G, Jensen RV, McCarter LL, et al. OpaR
715 Controls a Network of Downstream Transcription Factors in *Vibrio parahaemolyticus*
716 BB22OP. PLoS ONE. 2015;10(4):e0121863.

717 12. Papenfort K, Förstner KU, Cong JP, Sharma CM, Bassler BL. Differential RNA-seq of *Vibrio*
718 *cholerae* identifies the VqmR small RNA as a regulator of biofilm formation. Proc Natl Acad
719 Sci USA. 2015;112(7):E766–75.

720 13. Papenfort K, Silpe JE, Schramma KR, Cong JP, Seyedsayamdost MR, Bassler BL. A *Vibrio*
721 *cholerae* autoinducer–receptor pair that controls biofilm formation. Nat Chem Biol.
722 2017;13(5):551–7.

723 14. Boles BR, McCarter LL. *Vibrio parahaemolyticus scrABC* , a Novel Operon Affecting
724 Swarming and Capsular Polysaccharide Regulation. J Bacteriol. 2002;184(21):5946–54.

725 15. Ferreira RBR, Antunes LCM, Greenberg EP, McCarter LL. *Vibrio parahaemolyticus* ScrC
726 Modulates Cyclic Dimeric GMP Regulation of Gene Expression Relevant to Growth on
727 Surfaces. J Bacteriol. 2008;190(3):851–60.

728 16. Trimble MJ, McCarter LL. Bis-(3′-5′)-cyclic dimeric GMP-linked quorum sensing controls
729 swarming in *Vibrio parahaemolyticus*. Proc Natl Acad Sci USA. 2011;108(44):18079–84.

730 17. Lamb E, Trimble MJ, McCarter LL. Cell-cell communication, chemotaxis and recruitment in
731 *Vibrio parahaemolyticus*. Mol Microbiol. 2019;112(1):99–113.

732 18. Ferreira RBR, Chodur DM, Antunes LCM, Trimble MJ, McCarter LL. Output Targets and
733 Transcriptional Regulation by a Cyclic Dimeric GMP-Responsive Circuit in the *Vibrio*
734 *parahaemolyticus* Scr Network. J Bacteriol. 2012;194(5):914–24.

735 19. Kimbrough JH, Cribbs JT, McCarter LL. Homologous c-di-GMP-Binding Scr Transcription
736 Factors Orchestrate Biofilm Development in *Vibrio parahaemolyticus*. J Bacteriol.
737 2020;202(6):e00723-19.

738 20. Kim YK, McCarter LL. ScrG, a GGDEF-EAL Protein, Participates in Regulating Swarming
739 and Sticking in *Vibrio parahaemolyticus*. J Bacteriol. 2007;189(11):4094–107.

740 21. Kimbrough JH, McCarter LL. Identification of Three New GGDEF and EAL Domain-
741 Containing Proteins Participating in the Scr Surface Colonization Regulatory Network in
742 *Vibrio parahaemolyticus*. J Bacteriol. 2021;203(4):e00409-20.

743 22. Martínez-Méndez R, Camacho-Hernández DA, Sulvarán-Guel E, Zamorano-Sánchez D. A
744 Trigger Phosphodiesterase Modulates the Global c-di-GMP Pool, Motility, and Biofilm
745 Formation in *Vibrio parahaemolyticus*. J Bacteriol. 2021;203(13):e00046-21.

746 23. Zhong X, Lu Z, Wang F, Yao N, Shi M, Yang M. Characterization of GefA, a GGEEF Domain-
747 Containing Protein That Modulates *Vibrio parahaemolyticus* Motility, Biofilm Formation, and
748 Virulence. Appl Environ Microbiol. 2022;88(6):e02239-21.

749 24. Zamorano-Sánchez D, Alejandre-Sixtos JE, Arredondo-Hernández A, Martínez-Méndez R.
750 OpaR Exerts a Dynamic Control over c-di-GMP Homeostasis and *cpsA* Expression in *Vibrio*
751 *parahaemolyticus* through Its Regulation of ScrC and the Trigger Phosphodiesterase TpdA.
752 Microbiol Spectr. 2023;11(3):e00872-23.

753 25. Stewart BJ, McCarter LL. Lateral Flagellar Gene System of *Vibrio parahaemolyticus*. J
754 Bacteriol. 2003;185(15):4508–18.

755 26. Güvener ZT, McCarter LL. Multiple Regulators Control Capsular Polysaccharide Production
756 in *Vibrio parahaemolyticus*. J Bacteriol. 2003;185(18):5431–41.

757 27. Jaques S, McCarter LL. Three New Regulators of Swarming in *Vibrio parahaemolyticus*. J
758 Bacteriol. 2006;188(7):2625–35.

759 28. Hall-Stoodley L, Costerton JW, Stoodley P. Bacterial biofilms: from the Natural environment
760 to infectious diseases. Nat Rev Microbiol. 2004;2(2):95–108.

29. Sauer K, Stoodley P, Goeres DM, Hall-Stoodley L, Burmølle M, Stewart PS, et al. The biofilm life cycle: expanding the conceptual model of biofilm formation. Nat Rev Microbiol. 2022;20(10):608–20.

30. Lwoff A. LYSOGENY. Bacteriol Rev. 1953;17(4):269–337.

31. Oppenheim AB, Kobiler O, Stavans J, Court DL, Adhya S. Switches in Bacteriophage Lambda Development. Annu Rev Genet. 2005;39(1):409–29.

32. Ofir G, Sorek R. Contemporary Phage Biology: From Classic Models to New Insights. Cell. 2018;172(6):1260–70.

33. Zeng L, Skinner SO, Zong C, Sippy J, Feiss M, Golding I. Decision Making at a Subcellular Level Determines the Outcome of Bacteriophage Infection. Cell. 2010;141(4):682–91.

34. Yao T, Coleman S, Nguyen TVP, Golding I, Igoshin OA. Bacteriophage self-counting in the presence of viral replication. Proc Natl Acad Sci USA. 2021;118(51):e2104163118.

35. Łobocka MB, Rose DJ, Plunkett G, Rusin M, Samojedny A, Lehnherr H, et al. Genome of Bacteriophage P1. J Bacteriol. 2004;186(21):7032–68.

36. Ravin NV. Replication and Maintenance of Linear Phage-Plasmid N15. Microbiol Spectr. 2015;3(1):3.1.03.

37. Roberts JW, Roberts CW, Craig NL. *Escherichia coli recA* gene product inactivates phage lambda repressor. Proc Natl Acad Sci USA. 1978;75(10):4714–8.

38. Little JW. Autodigestion of *lexA* and phage lambda repressors. Proc Natl Acad Sci USA. 1984;81(5):1375–9.

39. Silpe JE, Bassler BL. A Host-Produced Quorum-Sensing Autoinducer Controls a Phage Lysis-Lysogeny Decision. Cell. 2019;176(1–2):268-280.e13.

40. Laganenka L, Sander T, Lagonenko A, Chen Y, Link H, Sourjik V. Quorum Sensing and Metabolic State of the Host Control Lysogeny-Lysis Switch of Bacteriophage T1. mBio. 2019;10(5):e01884-19.

41. Silpe JE, Bassler BL. Phage-Encoded LuxR-Type Receptors Responsive to Host-Produced Bacterial Quorum-Sensing Autoinducers. mBio. 2019;10(2):e00638-19.

42. Silpe JE, Duddy OP, Bassler BL. Natural and synthetic inhibitors of a phage-encoded quorum-sensing receptor affect phage–host dynamics in mixed bacterial communities. Proc Natl Acad Sci USA. 2022;119(49):e2217813119.

43. Duddy OP, Silpe JE, Fei C, Bassler BL. Natural silencing of quorum-sensing activity protects *Vibrio parahaemolyticus* from lysis by an autoinducer-detecting phage. PLoS Genet. 2023;19(7):e1010809.

44. Labrie SJ, Samson JE, Moineau S. Bacteriophage resistance mechanisms. Nat Rev Microbiol. 2010;8(5):317–27.

45. Zhang H, Li L, Zhao Z, Peng D, Zhou X. Polar flagella rotation in *Vibrio parahaemolyticus* confers resistance to bacteriophage infection. Sci Rep. 2016;6(1):26147.

46. Fogg PCM, Rigden DJ, Saunders JR, McCarthy AJ, Allison HE. Characterization of the relationship between integrase, excisionase and antirepressor activities associated with a superinfecting Shiga toxin encoding bacteriophage. Nucleic Acids Res. 2011;39(6):2116–29.

47. Tague JG, Hong J, Kalburge SS, Boyd EF. Regulatory Small RNA Qrr2 Is Expressed Independently of Sigma Factor-54 and Can Function as the Sole Qrr Small RNA To Control Quorum Sensing in *Vibrio parahaemolyticus*. J Bacteriol. 2022;204(1):e00350-21.

48. Gode-Potratz CJ, Kustusch RJ, Breheny PJ, Weiss DS, McCarter LL. Surface sensing in *Vibrio parahaemolyticus* triggers a programme of gene expression that promotes colonization and virulence: Surface-responsive gene expression. Mol Microbiol. 2011;79(1):240–63.

49. Zamorano-Sánchez D, Xian W, Lee CK, Salinas M, Thongsomboon W, Cegelski L, et al. Functional Specialization in *Vibrio cholerae* Diguanylate Cyclases: Distinct Modes of Motility Suppression and c-di-GMP Production. mBio. 2019;10(2):e00670-19.

50. Bridges AA, Prentice JA, Fei C, Wingreen NS, Bassler BL. Quantitative input–output dynamics of a c-di-GMP signal transduction cascade in *Vibrio cholerae*. PLoS Biol. 2022;20(3):e3001585.

51. Junkermeier EH, Hengge R. Local signaling enhances output specificity of bacterial c-di-GMP signaling networks. microLife. 2023;4:uqad026.

52. Erez Z, Steinberger-Levy I, Shamir M, Doron S, Stokar-Avihail A, Peleg Y, et al. Communication between viruses guides lysis–lysogeny decisions. Nature. 2017;541(7638):488–93.

53. Stokar-Avihail A, Tal N, Erez Z, Lopatina A, Sorek R. Widespread Utilization of Peptide Communication in Phages Infecting Soil and Pathogenic Bacteria. Cell Host Microbe. 2019;25(5):746-755.e5.

54. Aframian N, Omer Bendori S, Kabel S, Guler P, Stokar-Avihail A, Manor E, et al. Dormant phages communicate via arbitrium to control exit from lysogeny. Nat Microbiol. 2021;7(1):145–53.

55. Zhang Y, Qiu Y, Gao H, Sun J, Li X, Zhang M, et al. OpaR Controls the Metabolism of c-di-GMP in *Vibrio parahaemolyticus*. Front Microbiol. 2021;12:676436.

56. Chou SH, Galperin MY. Diversity of Cyclic Di-GMP-Binding Proteins and Mechanisms. J Bacteriol. 2016;198(1):32–46.

57. McCarter LL. Dual Flagellar Systems Enable Motility under Different Circumstances. Microb Physiol. 2004;7(1–2):18–29.

58. Lu R, Sun J, Qiu Y, Zhang M, Xue X, Li X, et al. The quorum sensing regulator OpaR is a repressor of polar flagellum genes in *Vibrio parahaemolyticus*. J Microbiol. 2021;59(7):651–7.

833 59. Yu Z, Schwarz C, Zhu L, Chen L, Shen Y, Yu P. Hitchhiking Behavior in Bacteriophages
834 Facilitates Phage Infection and Enhances Carrier Bacteria Colonization. Environ Sci Technol.
835 2021;55(4):2462–72.

836 60. You X, Kallies R, Kühn I, Schmidt M, Harms H, Chatzinotas A, et al. Phage co-transport with
837 hyphal-riding bacteria fuels bacterial invasion in a water-unsaturated microbial model system.
838 ISME J. 2022;16(5):1275–83.

839 61. Kolodkin-Gal I, Hazan R, Gaathon A, Carmeli S, Engelberg-Kulka H. A Linear Pentapeptide
840 Is a Quorum-Sensing Factor Required for *mazEF* -Mediated Cell Death in *Escherichia coli*.
841 Science. 2007;318(5850):652–5.

842 62. Kumar S, Kolodkin-Gal I, Engelberg-Kulka H. Novel Quorum-Sensing Peptides Mediating
843 Interspecies Bacterial Cell Death. mBio. 2013;4(3):e00314-13.

844 63. Høyland-Kroghsbo NM, Mærkedahl RB, Svenningsen SL. A Quorum-Sensing-Induced
845 Bacteriophage Defense Mechanism. mBio. 2013;4(1):e00362-12.

846 64. Tan D, Svenningsen SL, Middelboe M. Quorum Sensing Determines the Choice of Antiphage
847 Defense Strategy in *Vibrio anguillarum*. mBio. 2015;6(3):e00627-15.

848 65. Patterson AG, Jackson SA, Taylor C, Evans GB, Salmond GPC, Przybilski R, et al. Quorum
849 Sensing Controls Adaptive Immunity through the Regulation of Multiple CRISPR-Cas
850 Systems. Mol Cell. 2016;64(6):1102–8.

851 66. Hoque MM, Naser IB, Bari SMN, Zhu J, Mekalanos JJ, Faruque SM. Quorum Regulated
852 Resistance of *Vibrio cholerae* against Environmental Bacteriophages. Sci Rep.
853 2016;6(1):37956.

854 67. Moreau P, Diggle SP, Friman VP. Bacterial cell-to-cell signaling promotes the evolution of
855 resistance to parasitic bacteriophages. Ecol Evol. 2017;7(6):1936–41.

856 68. Høyland-Kroghsbo NM, Paczkowski J, Mukherjee S, Broniewski J, Westra E, Bondy-Denomy
857 J, et al. Quorum sensing controls the *Pseudomonas aeruginosa* CRISPR-Cas adaptive
858 immune system. Proc Natl Acad Sci USA. 2017;114(1):131–5.

859 69. Shah M, Taylor VL, Bona D, Tsao Y, Stanley SY, Pimentel-Elardo SM, et al. A phage-encoded
860 anti-activator inhibits quorum sensing in *Pseudomonas aeruginosa*. Mol Cell.
861 2021;81(3):571-583.e6.

862 70. Ghosh D, Roy K, Williamson KE, Srinivasiah S, Wommack KE, Radosevich M. Acyl-
863 Homoserine Lactones Can Induce Virus Production in Lysogenic Bacteria: an Alternative
864 Paradigm for Prophage Induction. Appl Environ Microbiol. 2009;75(22):7142–52.

865 71. Rossmann FS, Racek T, Wobser D, Puchalka J, Rabener EM, Reiger M, et al. Phage-
866 mediated Dispersal of Biofilm and Distribution of Bacterial Virulence Genes Is Induced by
867 Quorum Sensing. PLoS Pathog. 2015;11(2):e1004653.

868 72. Tan D, Hansen MF, De Carvalho LN, Røder HL, Burmølle M, Middelboe M, et al. High cell
869 densities favor lysogeny: induction of an H20 prophage is repressed by quorum sensing and
870 enhances biofilm formation in *Vibrio anguillarum*. ISME J. 2020;14(7):1731–42.

871 73. Li C, Wen A, Shen B, Lu J, Huang Y, Chang Y. FastCloning: a highly simplified, purification-
872 free, sequence- and ligation-independent PCR cloning method. BMC Biotechnol.
873 2011;11(1):92.

874 74. Sprouffske K, Wagner A. Growthcurver: an R package for obtaining interpretable metrics from
875 microbial growth curves. BMC Bioinform. 2016;17(1):172.

876

ACKNOWLEDGEMENTS

We are grateful to all members of the Bassler Laboratory for insightful discussion, and we thank Ned Wingreen for critical advice regarding quantitative aspects of the assays developed here.

880 **FIGURES & LEGENDS**

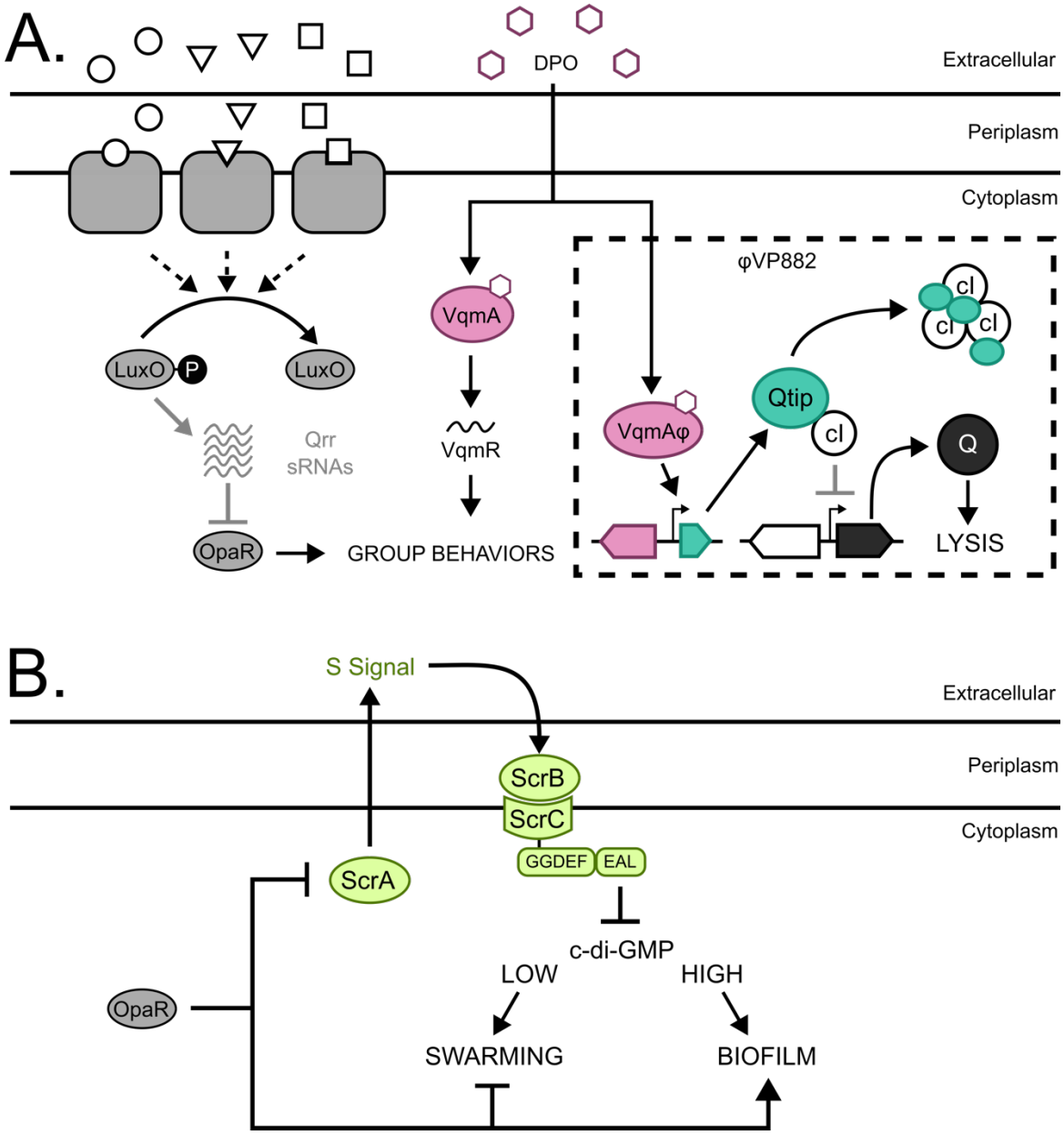

881

882 **Figure 1. *V. parahaemolyticus* QS controls φVP882 lysogeny-lysis transitions and surface**
883 **sensing.** (A) Schematic of *V. parahaemolyticus* QS pathways and their known interactions with
884 φVP882. Proteins involved in the LuxO-OpaR cascade are shown in gray. The circles, squares,
885 and triangles represent the autoinducers AI-1, AI-2, and CAI-1 that are recognized by their
886 corresponding receptors. At low cell density, autoinducers are sparse and LuxO is phosphorylated
887 (LuxO~P). LuxO~P activates expression of the genes encoding the Qrr sRNAs, and the Qrr
888 sRNAs repress *opaR*. At high cell density, LuxO is dephosphorylated and inactive. The Qrr sRNAs
889 are not made, and OpaR is produced. The DPO-VqmA QS pathway is shown in magenta. VqmA
890 bound to the DPO autoinducer (depicted as hexagons) activates expression of the gene encoding
891 the VqmR sRNA. OpaR and VqmR regulate genes underlying group behaviors. The dashed
892 square highlights φVP882 and its key regulatory components. The φVP882 homolog of host

893 VqmA, VqmAφ, also binds DPO, leading to production of Qtip, sequestration of the cI repressor,
894 de-repression of the antiterminator Q, and activation of the φVP882 lytic cycle. (B) Schematic of
895 the *V. parahaemolyticus* surface sensing pathway. Upon surface association, ScrA produces an
896 unknown molecule called the S-signal, which binds ScrB in the periplasm. ScrB in complex with
897 S-signal associates with ScrC on the inner membrane, triggering ScrC phosphodiesterase activity
898 which reduces the abundance of c-di-GMP and induces swarming motility. OpaR represses
899 *scrABC* and, thus, swarming motility. By contrast OpaR activates biofilm formation genes. GGDEF
900 and EAL denote the ScrC diguanylate cyclase and phosphodiesterase enzymatic activites,
901 respectively.
902

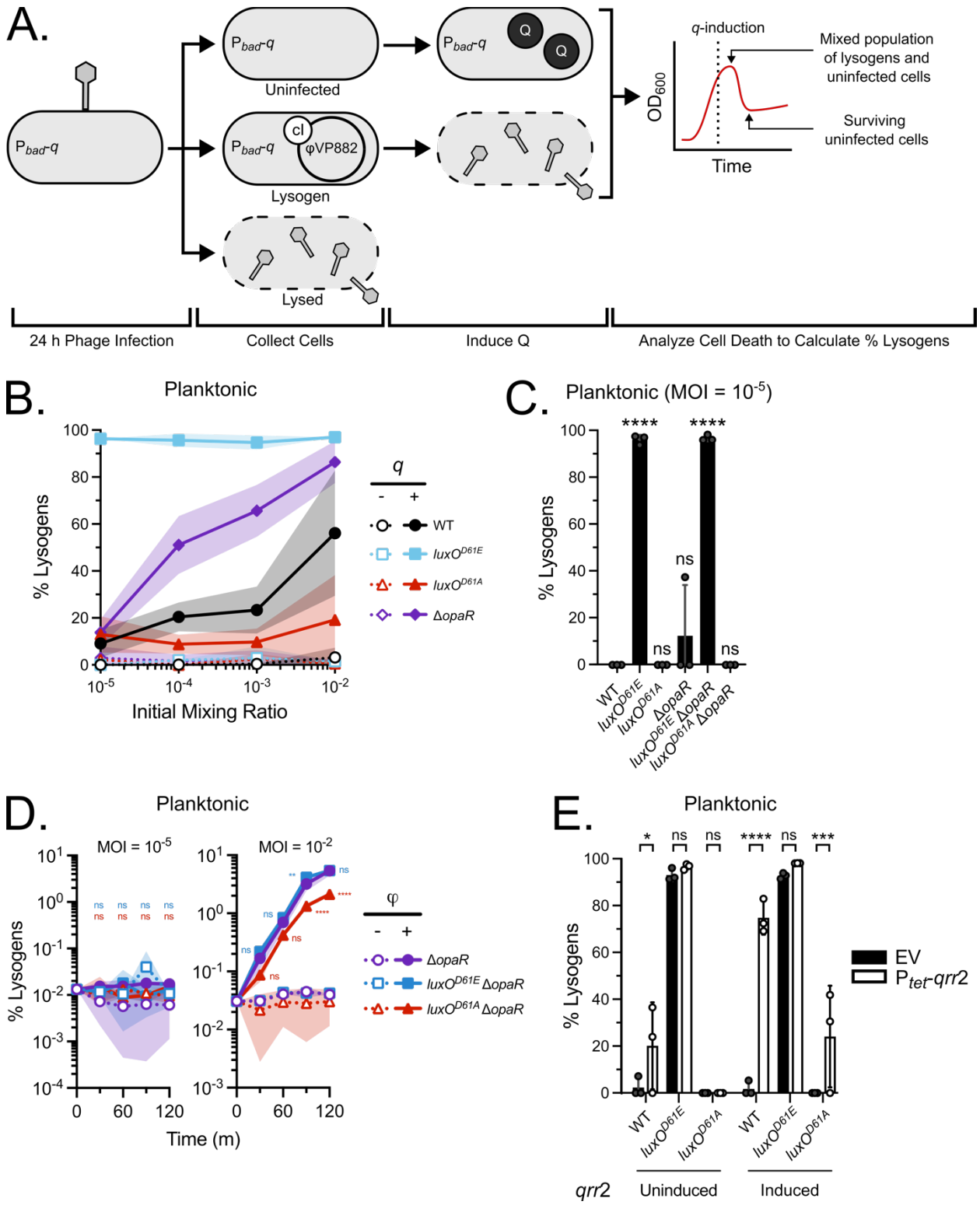

Figure 2. The Qrr sRNAs control φVP882 lysogenic conversion of planktonic *V. parahaemolyticus* RIMD strains. (A) Schematic of lysogenic conversion quantitation by *q*-induction. Following addition of φVP882 for 24 h to RIMD carrying P_{bad}-*q*, three outcomes are possible: Cells can remain uninfected or naïve (top), become infected and lysogenized (middle),

or become infected and lyse (bottom). Upon induction of *q* in the cells that survived infection, naïve cells remain unaffected while lysogenized cells lyse. Thus, cell death increases with the proportion of lysogens in each culture. The outcome of this assay is a peak and a subsequent valley in optical density of the culture (depicted in the theoretical plot on the right). The difference between the optical density values at the peak (total cells) and valley (remaining uninfected cells) can be used to determine the percentage of the population that has been lysogenized (see Materials and Methods). (B) Percent lysogens in the indicated planktonic strains at different MOIs. (C) Percent lysogens in the indicated planktonic strains. Infections were performed at MOI = 10^{-5}. (D) Lysogenic conversion over time in the indicated strains at (left) MOI = 10^{-5} and (right) MOI = 10^{-2}. Significance notations indicate comparisons between the *luxO*^{D61E} Δ*opaR* strain (blue) or the *luxO*^{D61A} Δ*opaR* strain (red) and the Δ*opaR* strain. (E) Percent lysogens in the indicated planktonic strains following overexpression of *qrr*2 (EV = empty vector, P_{tet}-*qrr*2 = inducible *qrr*2) during infection. Expression of *qrr*2 was uninduced (-aTc) or induced (+aTc). Infections were performed at MOI = 10^{-5}. (B-E) All experiments were performed in biological triplicate (n=3). (B,D) Lines and symbols represent the means and shaded areas represent the standard deviations. (C,E) Symbols represent individual replicate values. Bars represent the means. Error bars represent standard deviations. Results with *q*-induction (+arabinose) are shown. (C,D,E) Significance was determined by two-way ANOVA with Tukey's multiple comparisons test to determine adjusted p-values: (C) ns = non-significant, **** $p < 0.0001$, (D) ns = non-significant, ** $p = 0.0049$, **** $p < 0.0001$, (E) ns = non-significant, * $p = 0.0158$, *** $p = 0.0004$, **** $p < 0.0001$.

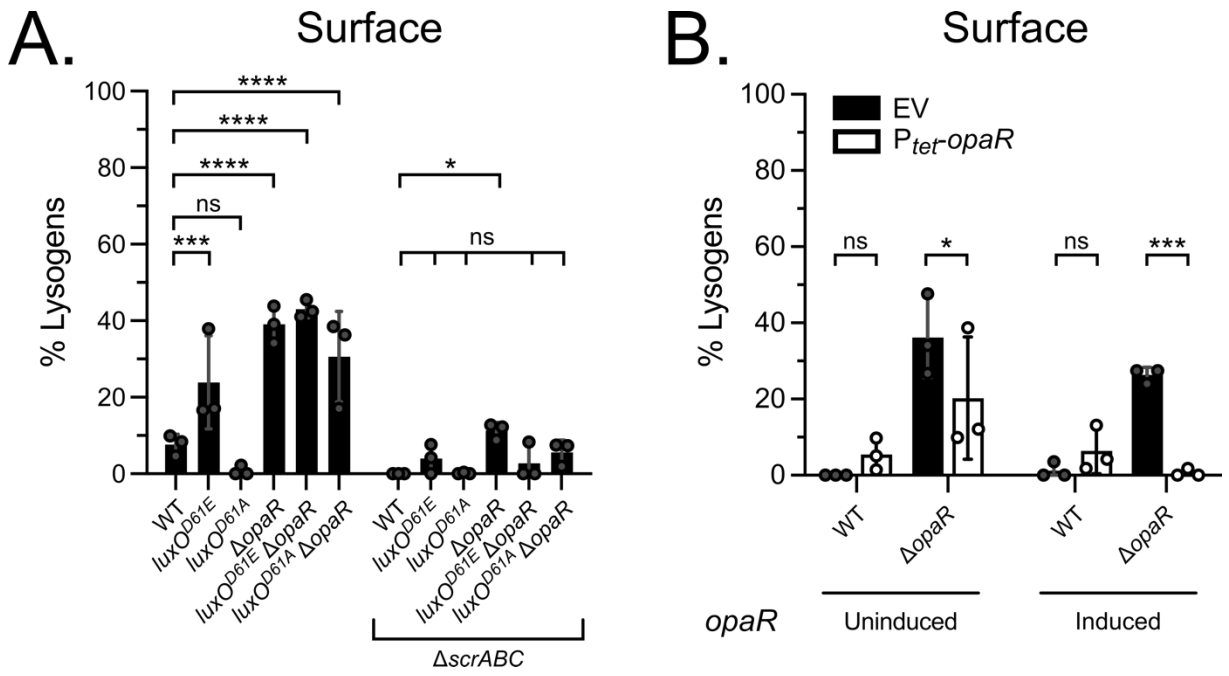

928

929 **Figure 3. OpaR suppresses φVP882 lysogenic conversion in surface-associated RIMD via**
930 **repression of the surface-sensing system encoded by *scrABC*.** (A) Percent lysogens in the
931 indicated surface-associated strains either containing or lacking the *scrABC* operon (Δ*scrABC*).
932 (B) Percent lysogens in the indicated strains following complementation with *opaR* (EV = empty
933 vector, P_{tet}-*opaR* = inducible *opaR*) during infection on a surface. *opaR* was uninduced (-aTc) or
934 induced (+aTc). (A,B) All experiments were performed in biological triplicate (n=3). Symbols
935 represent individual replicate values. Bars represent means. Error bars represent standard
936 deviations. Results with *q*-induction (+arabinose) are shown. Significance was determined by two-
937 way ANOVA with Tukey's multiple comparisons test to determine adjusted p-values: (A) ns = non-
938 significant, * p = 0.0376, *** p = 0.0007, **** p < 0.0001, (B) ns = non-significant, * p = 0.0327, ***
939 p = 0.0003.

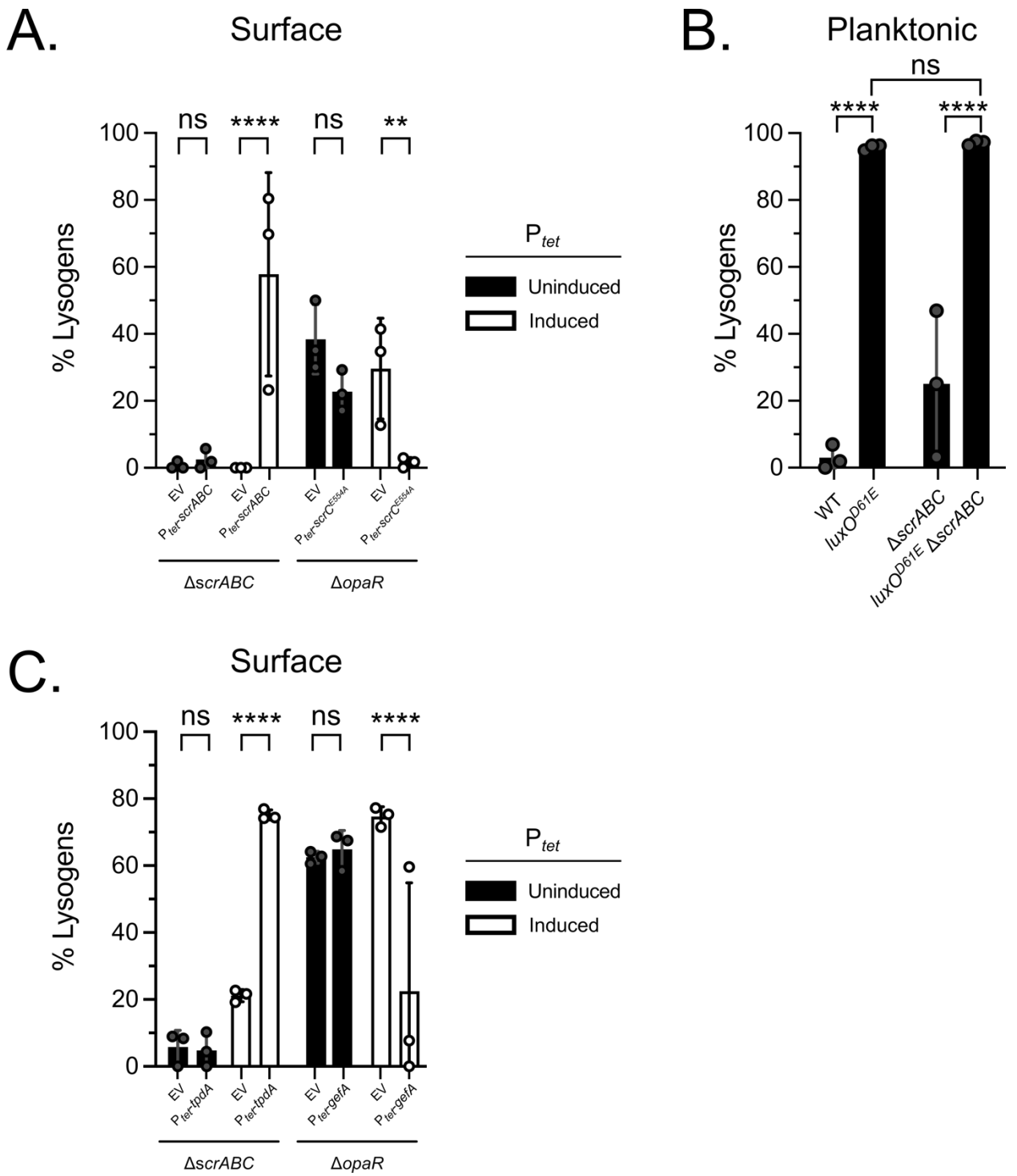

Figure 4. φVP882 lysogenic conversion of surface-associated RIMD host cells is regulated by the global c-di-GMP pool. (A) Percent lysogens in the indicated surface-associated strains without or with induction of *scrABC* (P_{tet}-*scrABC*; in this configuration ScrC functions as a phosphodiesterase) or $scrC^{E554A}$ (P_{tet}-$scrC^{E554A}$; a diguanylate cyclase) during infection. EV = empty vector control. (B) Percent lysogens in the indicated planktonic strains. (C) Percent lysogens in the indicated surface-associated strains without or with induction of *tpdA* (P_{tet}-*tpdA*; a phosphodiesterase) or *gefA* (P_{tet}-*gefA*; a diguanylate cyclase) during infection. EV = empty vector

control. (A-C) All experiments were performed in biological triplicate (n=3). Symbols represent individual replicate values. Bars represent means. Error bars represent standard deviations. Results with *q*-induction (+arabinose) are shown. (A,C) Expression from plasmids was uninduced (-aTc) or induced (+aTc). (A-C) Significance was determined by two-way ANOVA with Tukey's multiple comparisons test to determine adjusted p-values: (A) ns = non-significant, ** $p = 0.0054$, **** $p < 0.0001$, (B) ns = non-significant, **** $p < 0.0001$, (C) ns = non-significant, **** $p < 0.0001$.

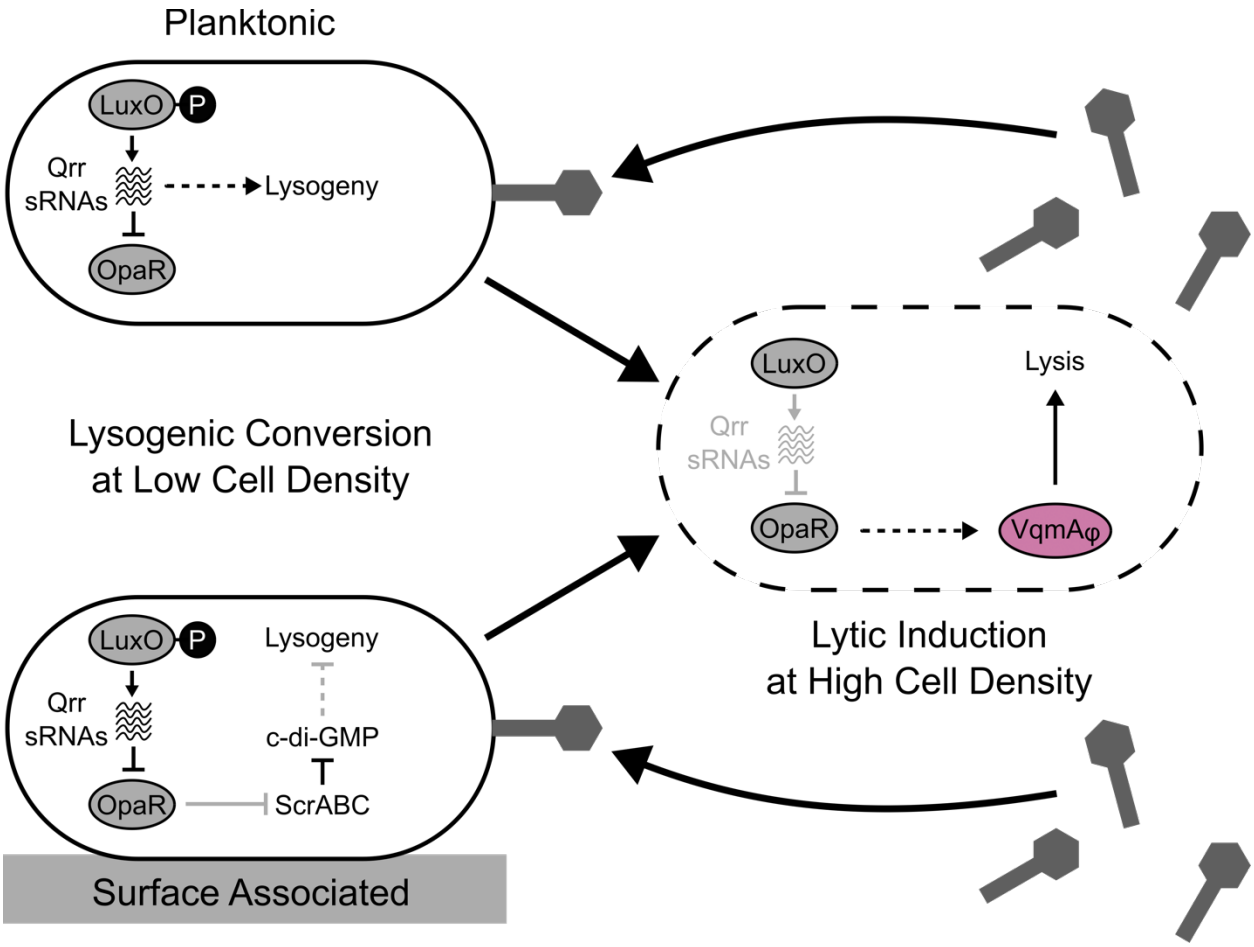

Figure 5. Regulation of φVP882 lysis-lysogeny transitions requires different QS components depending on the physical environment of the *V. parahaemolyticus* RIMD host. (Left) Schematics of the regulatory networks controlling φVP882 lysogenic conversion of low-cell-density host cells. (Top) In planktonic RIMD host cells, lysogenic conversion is driven by LuxO~P and the Qrr sRNAs in an OpaR-independent manner. (Bottom) In surface-associated RIMD host cells, LuxO~P drives derepression of *scrABC* and degradation of the c-di-GMP pool, promoting lysogenic conversion. (Right) Schematic of the known relationship between LuxO and the φVP882-encoded transcription factor and QS receptor VqmAφ (39,43). At high cell density, QS promotes lytic induction through a VqmAφ-dependent mechanism. (Left, Right) Solid and dashed arrows indicate direct and indirect regulation, respectively. Black and gray arrows indicate active and inactive regulatory pathways, respectively, under the specified physical conditions. Large arrows and phage particles indicate the φVP882 lifecycle.

1 **SUPPORTING INFORMATION**

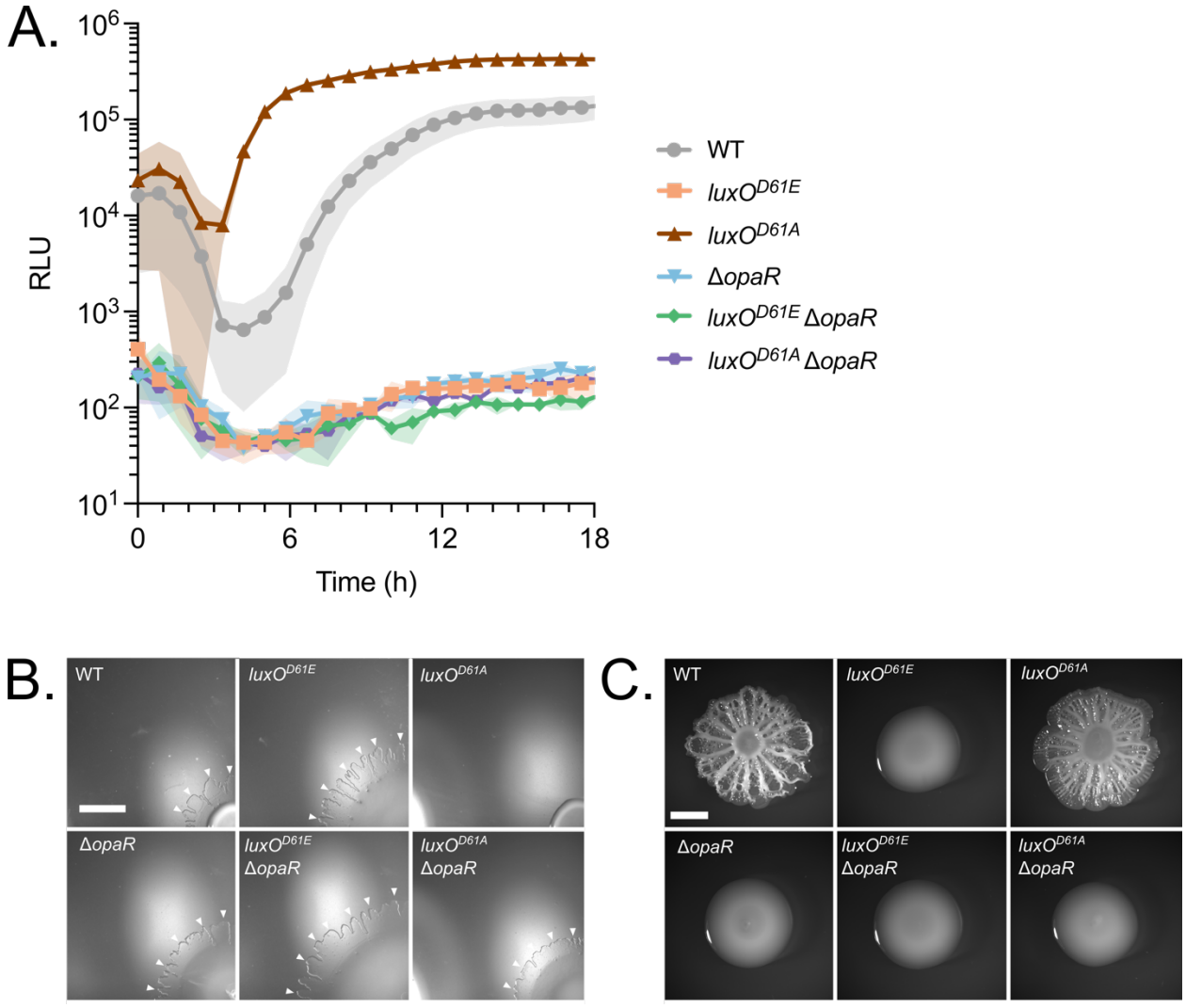

2

3 **S1 Fig. Phenotypic verification of RIMD QS mutants.** (A) Assessment of QS phenotypes in the
4 indicated strains carrying a QS-activated *lux* reporter (P_{luxC}-*luxCDABE*). Relative Light Units
5 (RLU) are bioluminescence normalized to OD_{600}. All experiments were performed in biological
6 triplicate (n=3). Lines and symbols represent the means and shaded areas represent the standard
7 deviations. (B) Representative stereoscope images of swarming morphologies of the indicated
8 strains 12 h post-inoculation. The bottom right corner of each image depicts the center of the
9 colony. White arrows indicate the outer edges of the swarm flares in the WT and low-cell-density-
10 locked strains. Swarming radius is measured from the bottom right corner of each image to the
11 edge of the swarm flare. (C) Representative stereoscope images of biofilm morphologies for the
12 indicated strains 42 h post-inoculation. (B,C) Scale bars = 3 mm. Swarming and biofilm
13 phenotypes for the strains mirror those reported in the literature (1).
14

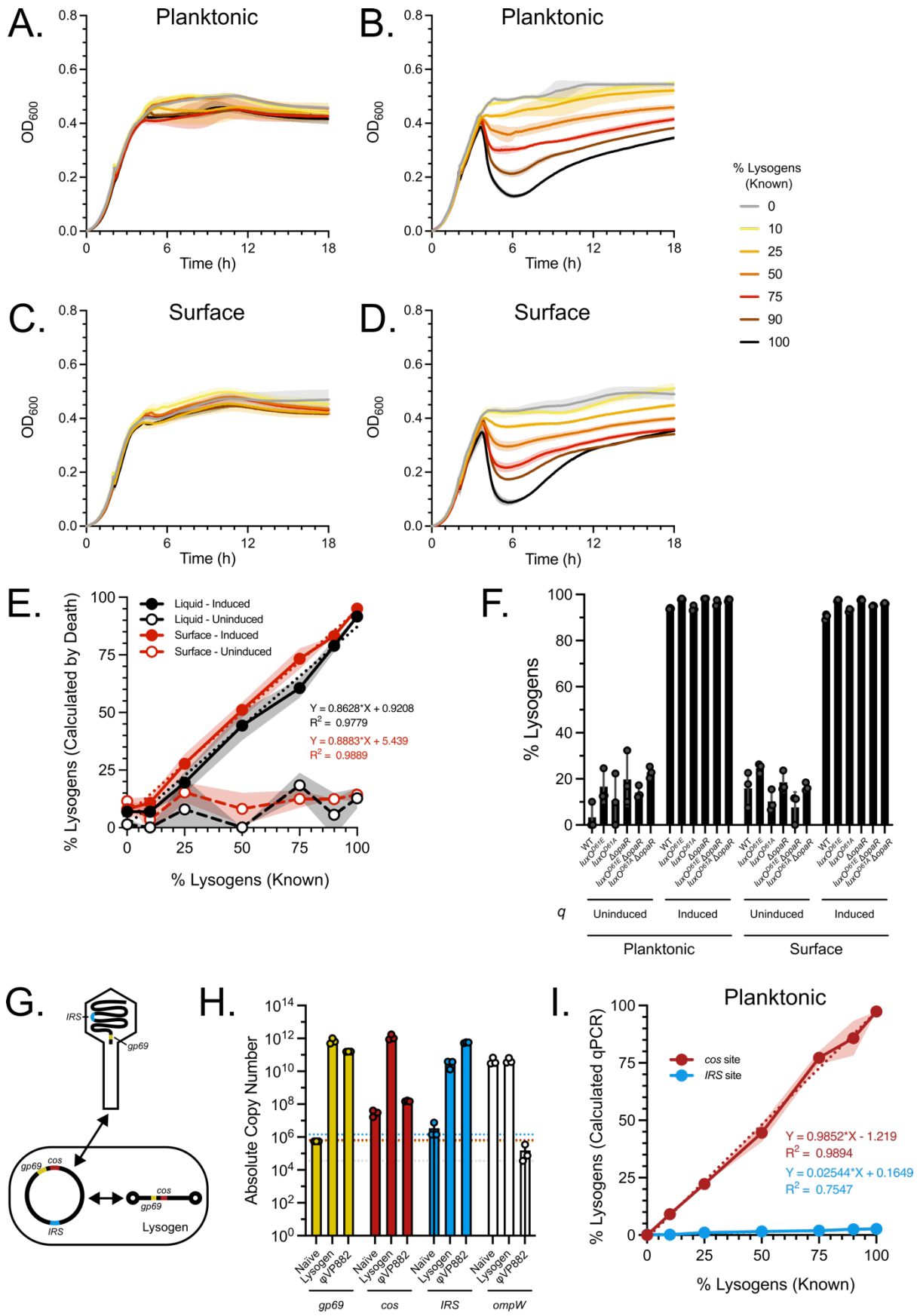
A.
Planktonic
B.
Planktonic
C.
Surface
D.
Surface
OD600
Time (h)
% Lysogens (Known)
0
10
25
50
75
90
100
E.
Liquid - Induced
Liquid - Uninduced
Surface - Induced
Surface - Uninduced
Y = 0.8628*X + 0.9208
R2 = 0.9779
Y = 0.8883*X + 5.439
R2 = 0.9889
% Lysogens (Calculated by Death)
% Lysogens (Known)
F.
% Lysogens
q
Uninduced
Induced
Uninduced
Induced
Planktonic
Surface
G.
IRS
gp69
cos
Lysogen
H.
Absolute Copy Number
Naive
Lysogen
φVP882
gp69
cos
IRS
ompW
I.
Planktonic
cos site
IRS site
Y = 0.9852*X - 1.219
R2 = 0.9894
Y = 0.02544*X + 0.1649
R2 = 0.7547
% Lysogens (Calculated qPCR)
% Lysogens (Known)

S2 Fig. Q-driven host cell lysis provides an accurate measure of lysogenic conversion in all test RIMD strains carrying φVP882. (A-D) Growth curves for WT RIMD populations consisting of known quantities of φVP882 lysogens and naïve host cells either (A,C) without *q*-induction (+dextrose) or (B,D) with *q*-induction (+arabinose). Strains were grown planktonically (A,B) or on a surface (C,D) prior to harvesting for the *q*-induction assay. Optical densities of samples in panels B and D at the peaks and valleys of their respective growth curves were used to calculate the lysogenized portion of the population (see Materials and Methods for a detailed explanation of the calculation). (E) Standard curves of the experimentally calculated percent lysogens versus the known percent lysogens without (+dextrose, open symbols) and with (+arabinose, closed symbols) *q*-induction for planktonically- (black) or surface-grown (red) cells. The dotted diagonal lines represent simple linear regressions performed on the induced samples. The resulting equations and R-squared values are shown. (F) Calculated percent lysogens in fully lysogenized populations of the indicated strains without (+dextrose) and with (+arabinose) *q*-induction after planktonic (left) or surface-associated (right) growth. (G) Diagram of the three genomic configurations of φVP882: the packaged linear form (top), the circular replicative form (bottom left), and the linear prophage form (bottom right). Shown are the *gp69* gene (yellow), the *cos* site (red), and the *IRS* (blue). Double-sided arrows represent the flow of genomic rearrangements. (H) Absolute quantitation of the indicated φVP882 genomic regions in naïve cells, lysogens, and purified φVP882 particles. *ompW* is a gene in the RIMD genome used to calculate host genome copy number. Dotted lines represent the limit of detection for the DNA region with the corresponding color. (I) Standard curve of percent lysogens calculated by qPCR using primers against the φVP882 *cos* site (red) versus the known percent lysogens. Primers targeting the φVP882 *IRS* (blue) were included to demonstrate that the circular replicative form of the φVP882 genome, which also contains an intact *cos* site, does not confound quantitation of φVP882 lysogens. The dotted diagonal lines represent simple linear regressions. The resulting equations and R-squared values are shown. (A-F,H,I) All experiments were performed in biological triplicate (n=3). (A-E,I) Lines and symbols represent the means, and shaded areas represent the standard deviations. (F,H) Symbols represent individual replicate values. Bars represent means. Error bars represent standard deviations.

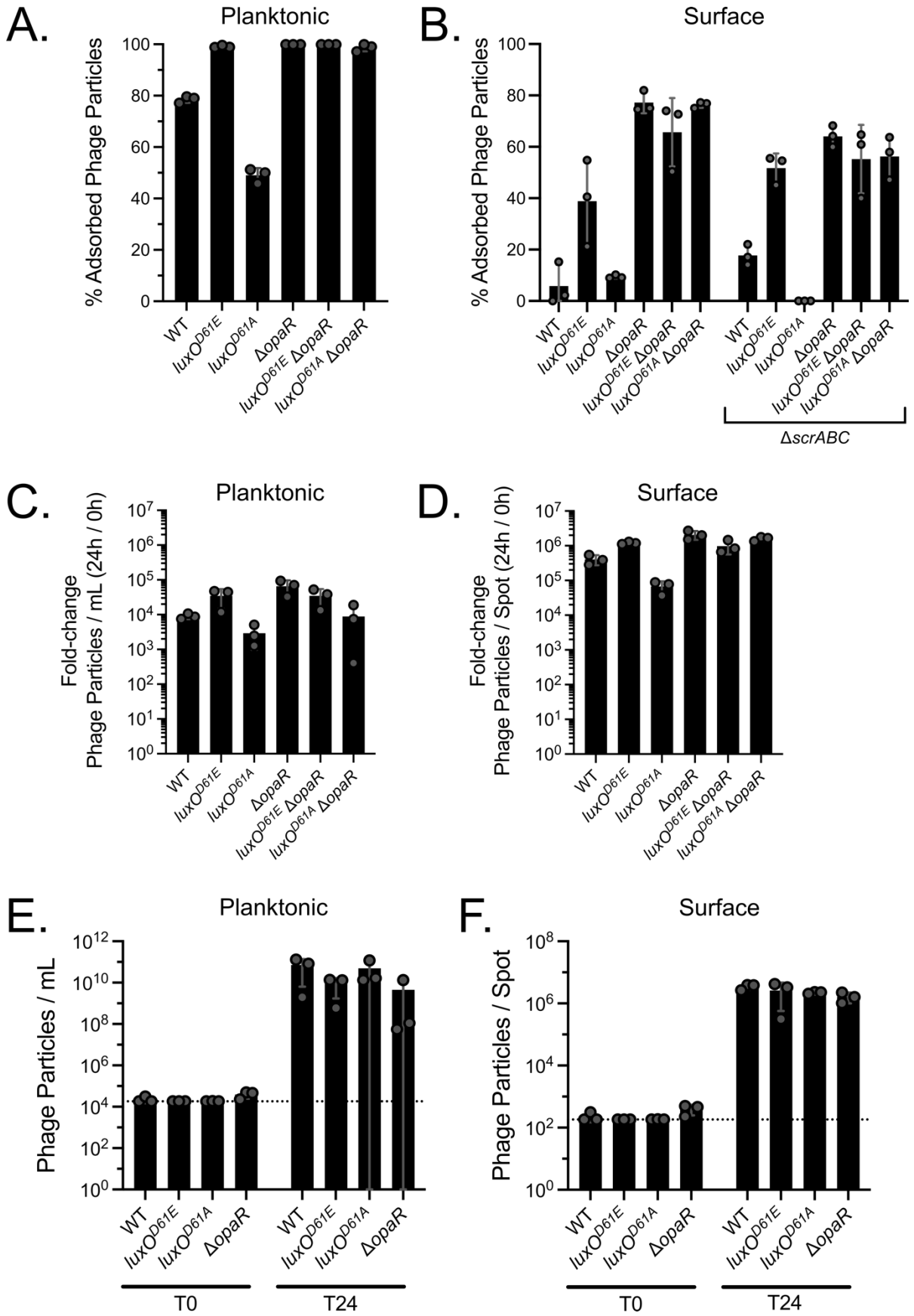
A.
Planktonic
% Adsorbed Phage Particles
100
80
60
40
20
0
WT
luxO^D61E
luxO^D61A
ΔopaR
luxO^D61E ΔopaR
luxO^D61A ΔopaR
B.
Surface
% Adsorbed Phage Particles
ΔscrABC
C.
Planktonic
Fold-change
Phage Particles / mL (24h / 0h)
D.
Surface
Fold-change
Phage Particles / Spot (24h / 0h)
E.
Planktonic
Phage Particles / mL
T0
T24
F.
Surface
Phage Particles / Spot

S3 Fig. φVP882 can adsorb to, infect, and undergo lytic replication in RIMD and all QS mutant strains in liquid and on a surface. (A,B) φVP882 adsorption to the indicated RIMD strains shown as the percentage of phage particles removed by the cells from the culture medium after growth (A) in liquid or (B) on a surface. In A,B data are shown as 100% - % recovered phage particles. (C,D) φVP882 viral particle production in the indicated strains after infection (C) in liquid or (D) on a surface. Data are shown as the fold-change in harvested free viral particles at the end (24 h) of the infection compared to that at the beginning (0 h). (E,F) Quantitation of phage particles produced spontaneously from the indicated lysogenic strains when grown (E) in liquid or (F) on a surface. Dotted line indicates the limit of detection by qPCR. (A-F) All experiments were performed in biological triplicate (n=3). Symbols represent individual replicate values. Bars represent means. Error bars represent standard deviations.

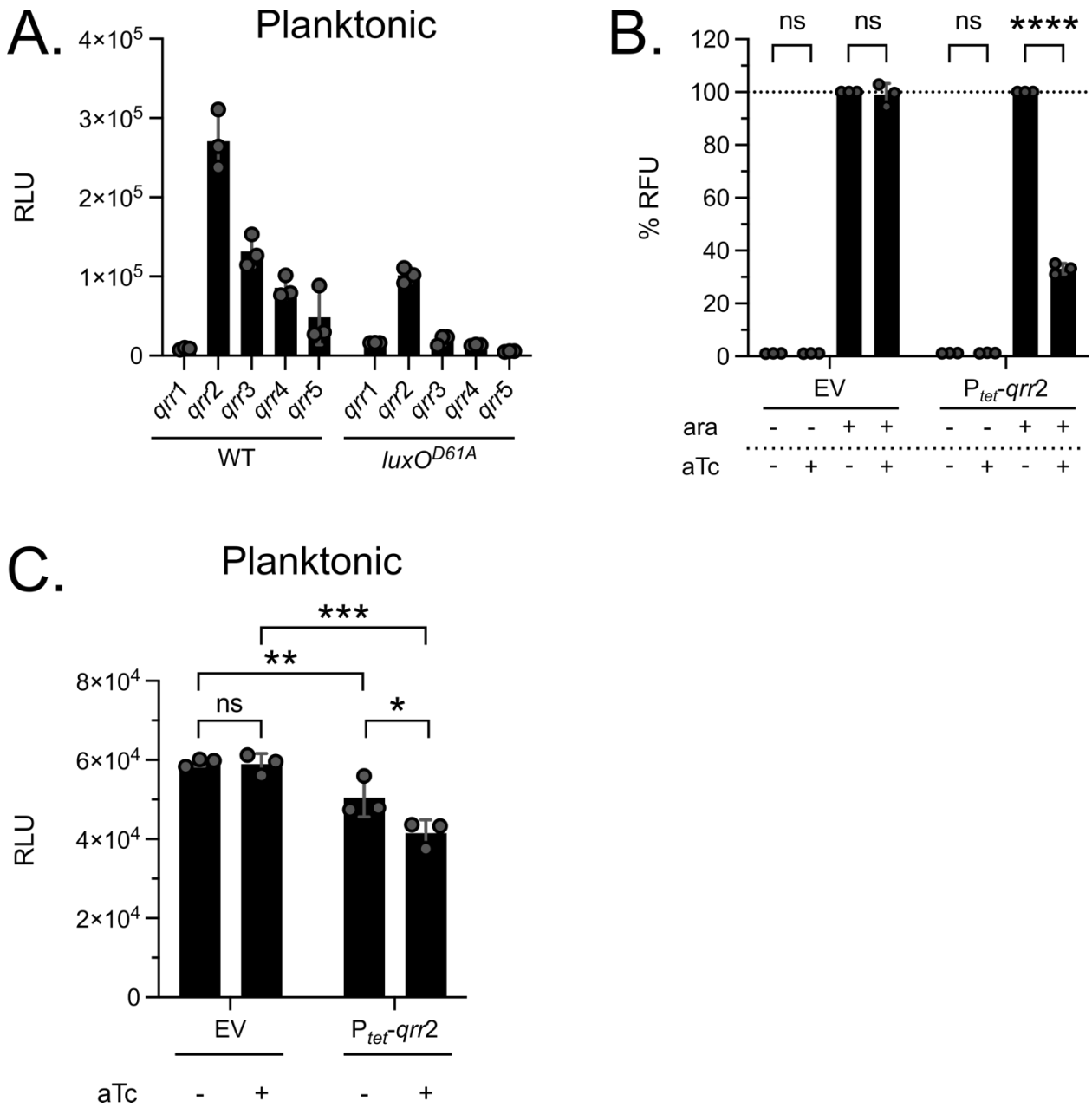

S4 Fig. The *qrr* sRNA genes are expressed, and the Qrr sRNAs are functional in *E. coli* and in RIMD. (A) Light production from transcriptional reporters of the five Qrr sRNA promoters ($P_{qrr1\text{-}5}$-*luxCDABE*) in WT RIMD and the high-cell-density-locked *luxO*^{D61A} strain during planktonic growth. (B) Fluorescence output is shown from *E. coli* strains carrying an *opaR-5'UTR-gfp* translational reporter (P_{bad}-*opaR-5'UTR-gfp*) and either an empty vector control (EV) or a *qrr*2 overexpression construct (P_{tet}-*qrr*2). The *opaR-5'UTR-gfp* translational reporter was uninduced (+dextrose) or induced (+arabinose) in the absence (-aTc) or presence (+aTc) of *qrr*2 overexpression. Data (% RFU) are represented as percent GFP signal for each sample compared to the sample following induction of only the *opaR-5'UTR-gfp* translational reporter. (C) Light production from a transcriptional reporter of a QS-activated promoter (P_{luxC}-*luxCDABE*) in RIMD carrying either an empty vector control (EV) or a *qrr*2 overexpression construct (P_{tet}-*qrr*2) is shown. Samples were uninduced (-aTc) or induced (+aTc). (A-C) All experiments were performed

in biological triplicate (n=3). Symbols represent individual replicate values. Bars represent means. Error bars represent standard deviations. (A,C) RLU are bioluminescence normalized to OD_{600}. (B,C) Significance was determined by two-way ANOVA with Tukey's multiple comparisons test to determine adjusted p-values: (B) ns = non-significant, **** $p < 0.0001$, (C) ns = non-significant, * $p = 0.0101$, ** $p = 0.0098$, *** $p = 0.0002$.

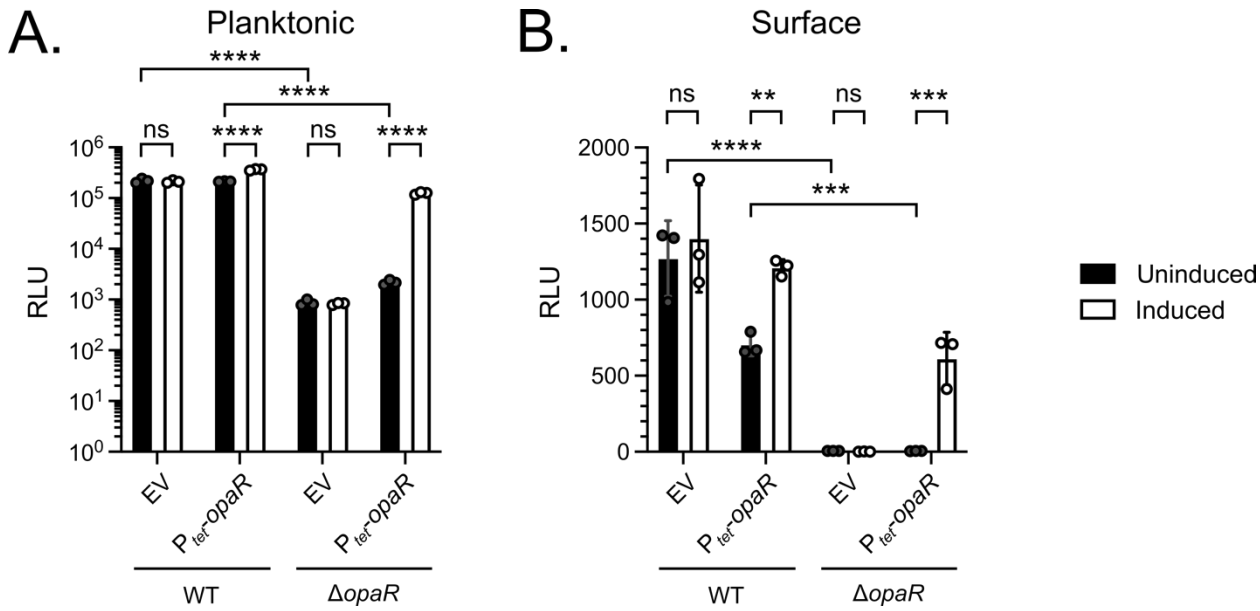

S5 Fig. OpaR produced from a plasmid functions in RIMD and can control high-cell-density behaviors in both planktonic and surface cultures. (A) Light production from a transcriptional reporter of the QS-activated luciferase operon (P_{luxC}-*luxCDABE*) in planktonic RIMD strains carrying either an empty vector control (EV) or an *opaR* overexpression construct (P_{tet}-*opaR*). (B) Light production from a transcriptional reporter of the QS-activated exopolysaccharide operon (P_{cpsA}-*luxCDABE*) in surface-associated RIMD strains carrying either EV or P_{tet}-*opaR*. (A,B) RLU are bioluminescence normalized to OD_{600}. All experiments were performed in biological triplicate (n=3). Symbols represent individual replicate values. Bars represent means. Error bars represent standard deviations. Samples were uninduced (-aTc, black) or induced (+aTc, white). Significance was determined by two-way ANOVA with Tukey's multiple comparisons test to determine adjusted p-values: (A) ns = non-significant, **** $p < 0.0001$, (B) ns = non-significant, ** $p = 0.0019$, *** $p = 0.0005$, 0.0004, **** $p < 0.0001$.

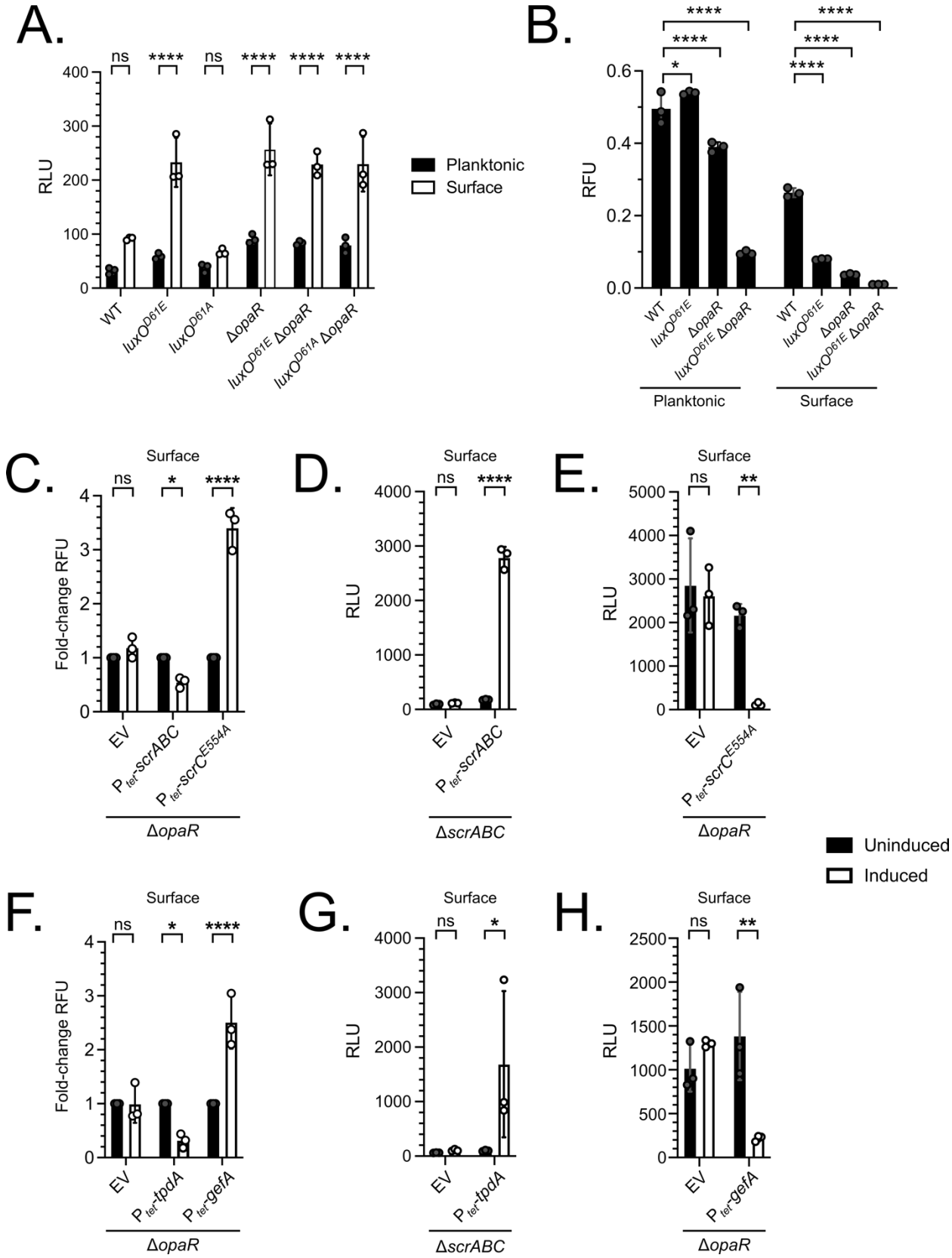
A.
ns
****
ns
****
****
****
RLU
400
300
200
100
0
WT
luxO^D61E
luxO^D61A
ΔopaR
luxO^D61E ΔopaR
luxO^D61A ΔopaR
Planktonic
Surface
B.
****
****
*
****
****
****
RFU
0.6
0.4
0.2
0.0
WT
luxO^D61E
ΔopaR
luxO^D61E ΔopaR
Planktonic
Surface
C.
Surface
ns
*
****
Fold-change RFU
EV
P tet-scrABC
P tet-scrC^E554A
ΔopaR
D.
Surface
ns
****
RLU
4000
3000
2000
1000
0
EV
P tet-scrABC
ΔscrABC
E.
Surface
ns
**
RLU
5000
4000
3000
2000
1000
0
EV
P tet-scrC^E554A
ΔopaR
Uninduced
Induced
F.
Surface
ns
*
****
Fold-change RFU
EV
P tet-tpdA
P tet-gefA
ΔopaR
G.
Surface
ns
*
RLU
4000
3000
2000
1000
0
EV
P tet-tpdA
ΔscrABC
H.
Surface
ns
**
RLU
2500
2000
1500
1000
500
0
EV
P tet-gefA
ΔopaR

94
95

S6 Fig. c-di-GMP abundance and surface behaviors can be modulated in surface-associated cultures with inducible expression of phosphodiesterases and diguanylate cyclases. (A) Light production from a transcriptional reporter of the *scrABC* surface sensing operon (P_{scrA}-*luxCDABE*) in planktonic (black) and surface-associated (white) RIMD strains. (B) Relative c-di-GMP abundance across the indicated strains grown either in liquid or on a solid surface. (C) Fold-change in c-di-GMP abundance in surface-associated Δ*opaR* RIMD carrying either an empty vector control (EV), an inducible *scrABC* operon (P_{tet}-*scrABC)* in which ScrC functions as a phosphodiesterase, or an inducible allele of *scrC* (P_{tet}-$scrC^{E554A}$) in which ScrC functions as a diguanylate cyclase. (D) Light production from a transcriptional reporter of the lateral flagellin promoter (P_{lafA}-*luxCDABE*) in surface-associated Δ*scrABC* RIMD carrying either EV or P_{tet}-*scrABC*. (E) Light production from P_{lafA}-*luxCDABE* in surface-associated Δ*opaR* RIMD carrying either EV or P_{tet}-$scrC^{E554A}$. (F) Fold-change in c-di-GMP abundance in surface-associated Δ*opaR* RIMD carrying either EV, an inducible P_{tet}-*tpdA* construct encoding the TpdA phosphodiesterase, or an inducible P_{tet}-*gefA* construct encoding the GefA diguanylate cyclase. (G) Light production from P_{lafA}-*luxCDABE* in surface-associated Δ*scrABC* RIMD carrying either EV or P_{tet}-*tpdA*. (H) Light production from P_{lafA}-*luxCDABE* in surface-associated Δ*opaR* RIMD carrying either EV or P_{tet}-*gefA*. (A-H) All experiments were performed in biological triplicate (n=3). Symbols represent individual replicate values. Bars represent means. Error bars represent standard deviations. (C-H) Black and white bars are uninduced (-aTc) and induced (+aTc), respectively. (A,D,E,G,H) RLU are bioluminescence normalized to OD_{600}. (B,C,F) RFU is c-di-GMP controlled TurboRFP fluorescence normalized to constitutive AmCyan fluorescence. (C,F) aTc-induced values (white) are represented as the fold-change versus their corresponding uninduced values (black). (A,C-G) Significance was determined by two-way ANOVA with Sidak's multiple comparisons test to determine adjusted p-values: (A) ns = non-significant, **** $p < 0.0001$, (C) ns = non-significant, * $p = 0.0232$, **** $p < 0.0001$, (D) ns = non-significant, **** $p < 0.0001$, (E) ns = non-significant, ** $p = 0.0095$, (F) ns = non-significant, * $p = 0.0168$, **** $p < 0.0001$, (G) ns = non-significant, * $p = 0.0395$, (H) ns = non-significant, ** $p = 0.0021$. (B) Significance was determined by two-way ANOVA with Tukey's multiple comparisons test to determine adjusted p-values: * $p = 0.0273$, **** $p < 0.0001$.

127 **S1 Table. Strains used in this study.**

Strain	Identifier	Genotype	Reference
V. parahaemolyticus O3 K6 RIMD 2210633 (RIMD)	FJS-S0045	Wildtype O3 K6 clinical isolate (WT, Sm^r)	(2)
	FJS-S0133	*luxO*^{D61E}	This study
	FJS-S0150	*luxO*^{D61A}	This study
	FJS-S0176	Δ*opaR*	This study
	FJS-S0178	*luxO*^{D61E} Δ*opaR*	This study
	FJS-S0445	*luxO*^{D61A} Δ*opaR*	This study
	FJS-S0277	Δ*cpsA*	This study
	FJS-S0279	Δ*cpsA luxO*^{D61E}	This study
	FJS-S0285	Δ*cpsA luxO*^{D61A}	This study
	FJS-S0281	Δ*cpsA* Δ*opaR*	This study
	FJS-S0283	Δ*cpsA luxO*^{D61E} Δ*opaR*	This study
	FJS-S0427	Δ*cpsA luxO*^{D61A} Δ*opaR*	This study
	FJS-S0289	Δ*cpsA* Δ*pomA*	This study
	FJS-S0291	Δ*cpsA* Δ*pomA luxO*^{D61E}	This study
	FJS-S0297	Δ*cpsA* Δ*pomA luxO*^{D61A}	This study
	FJS-S0293	Δ*cpsA* Δ*pomA* Δ*opaR*	This study
	FJS-S0295	Δ*cpsA* Δ*pomA luxO*^{D61E} Δ*opaR*	This study
	FJS-S0428	Δ*cpsA* Δ*pomA luxO*^{D61A} Δ*opaR*	This study
	FJS-S0946	Δ*cpsA*/pEVS143-P_{luxC}-*luxCDABE*	This study
	FJS-S0947	Δ*cpsA luxO*^{D61E}/pEVS143-P_{luxC}-*luxCDABE*	This study
	FJS-S0950	Δ*cpsA luxO*^{D61A}/pEVS143-P_{luxC}-*luxCDABE*	This study
	FJS-S0948	Δ*cpsA* Δ*opaR*/pEVS143-P_{luxC}-*luxCDABE*	This study
	FJS-S0949	Δ*cpsA luxO*^{D61E} Δ*opaR*/pEVS143-P_{luxC}-*luxCDABE*	This study

	FJS-S0951	Δ*cpsA luxO*^{D61A} Δ*opaR*/pEVS143-P$_{luxC}$-*luxCDABE*	This study
	FJS-S0553	Δ*cpsA* Δ*pomA*/pEVS143-P$_{bad}$-*q*	This study
	FJS-S0554	Δ*cpsA* Δ*pomA luxO*^{D61E}/pEVS143-P$_{bad}$-*q*	This study
	FJS-S0557	Δ*cpsA* Δ*pomA luxO*^{D61A}/pEVS143-P$_{bad}$-*q*	This study
	FJS-S0555	Δ*cpsA* Δ*pomA* Δ*opaR*/pEVS143-P$_{bad}$-*q*	This study
	FJS-S0556	Δ*cpsA* Δ*pomA luxO*^{D61E} Δ*opaR*/pEVS143-P$_{bad}$-*q*	This study
	FJS-S0558	Δ*cpsA* Δ*pomA luxO*^{D61A} Δ*opaR*/pEVS143-P$_{bad}$-*q*	This study
	FJS-S1033	Δ*cpsA* Δ*pomA*(φVP882::*cmR*)/pEVS143-P$_{bad}$-*q*	This study
	FJS-S1034	Δ*cpsA* Δ*pomA luxO*^{D61E}(φVP882::*cmR*)/pEVS143-P$_{bad}$-*q*	This study
	FJS-S1037	Δ*cpsA* Δ*pomA luxO*^{D61A}(φVP882::*cmR*)/pEVS143-P$_{bad}$-*q*	This study
	FJS-S1035	Δ*cpsA* Δ*pomA* Δ*opaR*(φVP882::*cmR*)/pEVS143-P$_{bad}$-*q*	This study
	FJS-S1036	Δ*cpsA* Δ*pomA luxO*^{D61E} Δ*opaR*(φVP882::*cmR*)/pEVS143-P$_{bad}$-*q*	This study
	FJS-S1038	Δ*cpsA* Δ*pomA luxO*^{D61A} Δ*opaR*(φVP882::*cmR*)/pEVS143-P$_{bad}$-*q*	This study
	FJS-S1151	Δ*cpsA* Δ*pomA*(φVP882)/pEVS143-P$_{bad}$-*q*	This study
	FJS-S1153	Δ*cpsA* Δ*pomA luxO*^{D61E}(φVP882)/pEVS143-P$_{bad}$-*q*	This study
	FJS-S1157	Δ*cpsA* Δ*pomA luxO*^{D61A}(φVP882)/pEVS143-P$_{bad}$-*q*	This study
	FJS-S1155	Δ*cpsA* Δ*pomA* Δ*opaR*(φVP882)/pEVS143-P$_{bad}$-*q*	This study

	FJS-S0843	Δ*cpsA* Δ*pomA*/pEVS143-P_{bad}-*q*/pXBCm	This study
	FJS-S0845	Δ*cpsA* Δ*pomA*/pEVS143-P_{bad}-*q*/pXBCm-*qrr*2	This study
	FJS-S0849	Δ*cpsA* Δ*pomA luxO*^{D61E}/pEVS143-P_{bad}-*q*/pXBCm	This study
	FJS-S0851	Δ*cpsA* Δ*pomA luxO*^{D61E}/pEVS143-P_{bad}-*q*/pXBCm-*qrr*2	This study
	FJS-S0855	Δ*cpsA* Δ*pomA luxO*^{D61A}/pEVS143-P_{bad}-*q*/pXBCm	This study
	FJS-S0857	Δ*cpsA* Δ*pomA luxO*^{D61A}/pEVS143-P_{bad}-*q*/pXBCm-*qrr*2	This study
	FJS-S1059	Δ*cpsA* Δ*pomA*/pEVS143-P_{qrr1}-*luxCDABE*	This study
	FJS-S1065	Δ*cpsA* Δ*pomA*/pEVS143-P_{qrr2}-*luxCDABE*	This study
	FJS-S1071	Δ*cpsA* Δ*pomA*/pEVS143-P_{qrr3}-*luxCDABE*	This study
	FJS-S1077	Δ*cpsA* Δ*pomA*/pEVS143-P_{qrr4}-*luxCDABE*	This study
	FJS-S1083	Δ*cpsA* Δ*pomA*/pEVS143-P_{qrr5}-*luxCDABE*	This study
	FJS-S1061	Δ*cpsA* Δ*pomA luxO*^{D61A}/pEVS143-P_{qrr1}-*luxCDABE*	This study
	FJS-S1067	Δ*cpsA* Δ*pomA luxO*^{D61A}/pEVS143-P_{qrr2}-*luxCDABE*	This study
	FJS-S1073	Δ*cpsA* Δ*pomA luxO*^{D61A}/pEVS143-P_{qrr3}-*luxCDABE*	This study
	FJS-S1079	Δ*cpsA* Δ*pomA luxO*^{D61A}/pEVS143-P_{qrr4}-*luxCDABE*	This study
	FJS-S1085	Δ*cpsA* Δ*pomA luxO*^{D61A}/pEVS143-P_{qrr5}-*luxCDABE*	This study
	FJS-S0988	Δ*cpsA*/pEVS143-P_{luxC}-*luxCDABE*/pXBCm	This study
	FJS-S0990	Δ*cpsA*/pEVS143-P_{luxC}-*luxCDABE*/pXBCm-*qrr*2	This study
	FJS-S0565	Δ*cpsA* Δ*pomA* Δ*scrABC*/pEVS143-P_{bad}-*q*	This study

	FJS-S0566	Δ*cpsA* Δ*pomA* Δ*scrABC* *luxO*^{D61E}/pEVS143-P$_{bad}$-*q*	This study
	FJS-S0569	Δ*cpsA* Δ*pomA* Δ*scrABC* *luxO*^{D61A}/pEVS143-P$_{bad}$-*q*	This study
	FJS-S0567	Δ*cpsA* Δ*pomA* Δ*scrABC* Δ*opaR*/pEVS143-P$_{bad}$-*q*	This study
	FJS-S0568	Δ*cpsA* Δ*pomA* Δ*scrABC* *luxO*^{D61E} Δ*opaR*/pEVS143-P$_{bad}$-*q*	This study
	FJS-S0570	Δ*cpsA* Δ*pomA* Δ*scrABC* *luxO*^{D61A} Δ*opaR*/pEVS143-P$_{bad}$-*q*	This study
	FJS-S952	Δ*cpsA* Δ*pomA*/pEVS143-P$_{bad}$-*q*/pXBCm-*opaR*	This study
	FJS-S0883	Δ*cpsA* Δ*pomA* Δ*opaR*/pEVS143-P$_{bad}$-*q*/pXBCm	This study
	FJS-S0954	Δ*cpsA* Δ*pomA* Δ*opaR*/pEVS143-P$_{bad}$-*q*/pXBCm-*opaR*	This study
	FJS-S0994	Δ*cpsA*/pEVS143-P$_{luxC}$-*luxCDABE*/pXBCm-*opaR*	This study
	FJS-S0995	Δ*cpsA* Δ*opaR*/pEVS143-P$_{luxC}$-*luxCDABE*/pXBCm	This study
	FJS-S0996	Δ*cpsA* Δ*opaR*/pEVS143-P$_{luxC}$-*luxCDABE*/pXBCm-*opaR*	This study
	FJS-S0933	Δ*pomA* Δ*lacIZ*::P$_{tac}$-*mScarletI* /pEVS143-P$_{cpsA}$-*luxCDABE*/pXBCm	This study
	FJS-S0934	Δ*pomA* Δ*lacIZ*::P$_{tac}$-*mScarletI* /pEVS143-P$_{cpsA}$-*luxCDABE*/pXBCm-*opaR*	This study
	FJS-S0935	Δ*pomA* Δ*opaR* Δ*lacIZ*::P$_{tac}$-*mScarletI* /pEVS143-P$_{cpsA}$-*luxCDABE*/pXBCm	This study
	FJS-S0936	Δ*pomA* Δ*opaR* Δ*lacIZ*::P$_{tac}$-*mScarletI* /pEVS143-P$_{cpsA}$-*luxCDABE*/pXBCm-*opaR*	This study
	FJS-S0958	Δ*cpsA* Δ*pomA* Δ*scrABC*/pEVS143-P$_{bad}$-*q*/pXBCm	This study
	FJS-S0964	Δ*cpsA* Δ*pomA* Δ*scrABC*/pEVS143-P$_{bad}$-*q*/pXBCm-*scrABC*	This study
	FJS-S1031	Δ*cpsA* Δ*pomA* Δ*opaR*/pEVS143-P$_{bad}$-*q*/pXBCm-*scrC*^{E554A}	This study

	FJS-S1094	Δ*cpsA* Δ*pomA* Δ*scrABC*/pEVS143-P_{bad}-*q*/pXBCm-*tpdA*	This study
	FJS-S1095	Δ*cpsA* Δ*pomA* Δ*opaR*/pEVS143-P_{bad}-*q*/pXBCm-*gefA*	This study
	FJS-S0820	Δ*pomA* Δ*lacIZ*::P_{tac}-*mScarletI* /pEVS143-P_{scrA}-*luxCDABE*	This study
	FJS-S0821	Δ*pomA luxO*^{D61E} Δ*lacIZ*::P_{tac}-*mScarletI* /pEVS143-P_{scrA}-*luxCDABE*	This study
	FJS-S0824	Δ*pomA luxO*^{D61A} Δ*lacIZ*::P_{tac}-*mScarletI* /pEVS143-P_{scrA}-*luxCDABE*	This study
	FJS-S0822	Δ*pomA* Δ*opaR* Δ*lacIZ*::P_{tac}-*mScarletI* /pEVS143-P_{scrA}-*luxCDABE*	This study
	FJS-S0823	Δ*pomA luxO*^{D61E} Δ*opaR* Δ*lacIZ*::P_{tac}-*mScarletI* /pEVS143-P_{scrA}-*luxCDABE*	This study
	FJS-S0825	Δ*pomA luxO*^{D61A} Δ*opaR* Δ*lacIZ*::P_{tac}-*mScarletI* /pEVS143-P_{scrA}-*luxCDABE*	This study
	FJS-S0360	Δ*pomA*/pFY4535	This study
	FJS-S0362	Δ*pomA luxO*^{D61E}/pFY4535	This study
	FJS-S0364	Δ*pomA* Δ*opaR*/pFY4535	This study
	FJS-S0366	Δ*pomA luxO*^{D61E} Δ*opaR*/pFY4535	This study
	FJS-S1053	Δ*pomA* Δ*opaR*/pFY4535/pXBCm	This study
	FJS-S1054	Δ*pomA* Δ*opaR*/pFY4535/pXBCm-*scrABC*	This study
	FJS-S1055	Δ*pomA* Δ*opaR*/pFY4535/pXBCm-*scrC*^{E554A}	This study
	FJS-S1020	Δ*pomA* Δ*scrABC* Δ*lacIZ*::P_{tac}-*mScarletI*/pEVS143-P_{lafA}-*luxCDABE*/pXBCm	This study
	FJS-S1024	Δ*pomA* Δ*scrABC* Δ*lacIZ*::P_{tac}-*mScarletI*/pEVS143-P_{lafA}-*luxCDABE*/pXBCm-*scrABC*	This study
	FJS-S1019	Δ*pomA* Δ*opaR* Δ*lacIZ*::P_{tac}-*mScarletI*/pEVS143-P_{lafA}-*luxCDABE*/pXBCm	This study
	FJS-S1029	Δ*pomA* Δ*opaR* Δ*lacIZ*::P_{tac}-*mScarletI*/pEVS143-P_{lafA}-*luxCDABE*/pXBCm-*scrC*^{E554A}	This study

	FJS-S1098	Δ*pomA* Δ*scrABC* Δ*lacIZ*::P_{tac}-*mScarletI*/pEVS143-P_{lafA}-*luxCDABE*/pXBCm-*tpdA*	This study
	FJS-S1101	Δ*pomA* Δ*opaR* Δ*lacIZ*::P_{tac}-*mScarletI*/pEVS143-P_{lafA}-*luxCDABE*/pXBCm-*gefA*	This study
V. parahaemolyticus O3 K6 882	FJS-S0018	Wildtype φVP882 lysogen	(3)
	BB-Vp0004	(φVP882)/pEVS143-P_{bad}-*vqmAφ*	(4)
E. coli TOP10	FJS-S0970	/pEVS143-P_{bad}-*opaR-5'UTR-gfp*/pXBCm	This study
	FJS-S0972	/pEVS143-P_{bad}-*opaR-5'UTR-gfp*/pXBCm-*qrr2*	This study

128

129

130 **S2 Table. Primers and Synthesized Fragments used in this study.**

Primer*	Sequence**	Description/Associated construct
FJS-O132	agtgaactgcatgaattcccGTGGAAGCAATGACCATG	Forward primer for upstream homology arm for the *cpsA* deletion / pRE112-Δ*cpsA*
FJS-O133	cgccgccttaCATGACCTAGTTTCCCTTC	Reverse primer for upstream homology arm for the *cpsA* deletion / pRE112-Δ*cpsA*
FJS-O134	ctaggtcatgTAAGGCGGCGATGATGAAAAC	Forward primer for downstream homology arm for the *cpsA* deletion / pRE112-Δ*cpsA*
FJS-O135	atgcgatatcgagctctcccGCTGTTCCAATCGTGTTTG	Reverse primer for downstream homology arm for the *cpsA* deletion / pRE112-Δ*cpsA*
FJS-O138	GCCGTACACTAGTATCACAACC	Forward primer for verification of the *cpsA* deletion
FJS-O139	CACGACTAAACGATGACGATGA	Reverse primer for verification of the *cpsA* deletion
FJS-O018	agtgaactgcatgaattcccATGCTTGGCCGACACACATG	Forward primer for upstream homology arm for the *pomA* deletion / pRE112-Δ*pomA*
FJS-O019	tccgcgattaCACAAAGCACTCCTCACGC	Reverse primer for upstream homology arm for the *pomA* deletion / pRE112-Δ*pomA*
FJS-O020	gtgctttgtgTAATCGCGGAGATTTGTG	Forward primer for downstream homology arm for the *pomA* deletion / pRE112-Δ*pomA*
FJS-O021	atgcgatatcgagctctcccTTTATCTTCTGAACTATTTTATAGACG	Reverse primer for downstream homology arm for the *pomA* deletion / pRE112-Δ*pomA*
FJS-O022	ATAGCGTGAGGAGTGCTTTG	Forward primer for verification of the *pomA* deletion
FJS-O023	GGCGTGTGAGTCAGGATTT	Reverse primer for verification of the *pomA* deletion
FJS-O036	agtgaactgcatgaattcccCTTAGTGGGTATCAACTTGC	Forward primer for upstream homology arm for the *luxO* point mutants / pRE112-*luxO*^{D61x}
FJS-O037	gacgaagctcGAGAAGAATAAGATCTGGAATTCG	Reverse primer for upstream homology arm for the *luxO*^{D61E} point mutant / pRE112-*luxO*^{D61E}

FJS-O040	gacgaagtgcGAGAAGAATAAGATCTGGAATTCG	Reverse primer for upstream homology arm for the *luxO*^{D61A} point mutant / pRE112-*luxO*^{D61A}
FJS-O038	tattcttctcgagCTTCGTCTGCCAGATATGAC	Forward primer for downstream homology arm for the *luxO*^{D61E} point mutant / pRE112-*luxO*^{D61E}
FJS-O041	tattcttctcgcaCTTCGTCTGCCAGATATGAC	Forward primer for downstream homology arm for the *luxO*^{D61A} point mutant / pRE112-*luxO*^{D61A}
FJS-O039	atgcgatatcgagctctcccGCTCAATCAGTTTAGATACAGATG	Reverse primer for downstream homology arm for the *luxO* point mutants / pRE112-*luxO*^{D61x}
FJS-O067	GCTTTTTAGCGCATGGCTGATCTC	Forward primer for verification of the *luxO* point mutants
FJS-O068	GAGGGGTCGCTAATATATCAGCATGC	Reverse primer for verification of the *luxO* point mutants
FJS-O046	agtgaactgcatgaattcccAGACCGTTGAAGCATCGTAC	Forward primer for upstream homology arm for the *opaR* deletion / pRE112-Δ*opaR*
FJS-O047	ctgagctttaCATATCCATTTTCCTTGCCATTTG	Reverse primer for upstream homology arm for the *opaR* deletion / pRE112-Δ*opaR*
FJS-O048	aatggatatgTAAAGCTCAGATTTGAACACG	Forward primer for downstream homology arm for the *opaR* deletion / pRE112-Δ*opaR*
FJS-O049	atgcgatatcgagctctcccGGTCTAGAAATGGGTACGG	Reverse primer for downstream homology arm for the *opaR* deletion / pRE112-Δ*opaR*
FJS-O050	GATACCAACACCAACAACGAAC	Forward primer for verification of the *opaR* deletion
FJS-O051	CAATCACTGACCTGCCAAATAAA	Reverse primer for verification of the *opaR* deletion
FJS-O199	gcggtgtaagtgaactgcatgaattcccTGATTATCACCGCCAGCATG	Forward primer for upstream homology arm for the *scrABC* deletion / pRE112-Δ*scrABC*
FJS-O200	attgaaagaagttaCATTTTTTTCGATCCTTGTCGG	Reverse primer for upstream homology arm for the *scrABC* deletion / pRE112-Δ*scrABC*
FJS-O201	gatcgaaaaaaatgTAACTTCTTTCAATACAACCTC	Forward primer for downstream homology arm for the *scrABC* deletion / pRE112-Δ*scrABC*

FJS-O202	ggtaccgcatgcgatatcgagctctcccTCAATCACTTCCGCTTTAC	Reverse primer for downstream homology arm for the *scrABC* deletion / pRE112-Δ*scrABC*
FJS-O234	GACCGTGAGTTGCGATGTAA	Forward primer for verification of the *scrABC* deletion
FJS-O235	GGCTTGCTGTTGAGAGGTAA	Reverse primer for verification of the *scrABC* deletion
FJS-O329	AATTCGATATCAAGCTTATCGATAC	Forward primer for generation of linearized pXBCm
FJS-O330	AGCTCCCATTTCACTTTTC	Reverse primer for generation of linearized pXBCm
FJS-O337	tcagtgatagagaaaagtgaaatgggagctCGACCCTTCTTAAGCCGAG	Forward primer for insertion of the *qrr*2 gene into pXBCm
FJS-O338	cgacggtatcgataagcttgatatcgaattTAAATCAAATAACCTTAGTAAAGAAATGG	Reverse primer for insertion of the *qrr*2 gene into pXBCm
FJS-O387	tcagtgatagagaaaagtgaaatgggagct**gtacaggaggtgtgaa**ATGGACTCAATTGCAAAGAG	Forward primer for insertion of the *opaR* gene into pXBCm
FJS-O388	cgacggtatcgataagcttgatatcgaattTTAGTGTTCGCGATTGTAGATG	Reverse primer for insertion of the *opaR* gene into pXBCm
FJS-O345	tcagtgatagagaaaagtgaaatgggagct**gtacaggaggtgtgaa**ATGAGCGACAAGGATTCTATTC	Forward primer for insertion of the *scrABC* genes into pXBCm
FJS-O346	cgacggtatcgataagcttgatatcgaattTTATGACCAAGTAGGTTGGTTTAG	Reverse primer for insertion of the *scrABC* genes into pXBCm
FJS-O389	tcagtgatagagaaaagtgaaatgggagct**gtacaggaggtgtgaa**ATGAAAAAGGCTGTTAAAAAAATATC	Forward primer for insertion of the *scrC* gene into pXBCm
FJS-O410	ccaacgcatcaat<u>gc</u>TGCTGCGCCAACAATTTTG	Reverse primer to generate *scrC*^{E554A}
FJS-O411	attgttggcgca<u>gca</u>GCATTGATGCGTTGGAATG	Forward primer to generate *scrC*^{E554A}
FJS-O390	cgacggtatcgataagcttgatatcgaattTTATGACCAAGTAGGTTGGTTTAG	Reverse primer for insertion of the *scrC* gene into pXBCm
FJS-O442	agaaaagtgaaatgggagct**gtacaggaggtgtgaa**ATGATTAGGTTTGAACTTGGAAAC	Forward primer for insertion of the *tpdA* gene into pXBCm
FJS-O443	cgacggtatcgataagcttgatatcgaattCTAGAAATGCAGAGGATAGAAG	Reverse primer for insertion of the *tpdA* gene into pXBCm
FJS-O440	gagaaaagtgaaatgggagct**gtacaggaggtgtgaa**ATGACTGACGAGTTTAAGAAATC	Forward primer for insertion of the *gefA* gene into pXBCm

FJS-O441	cgacggtatcgataagcttgatatcgaattTTAGATAGGCATCACTCGG	Reverse primer for insertion of the *gefA* gene into pXBCm
FJS-O062	ATGACTAAAAAAATTTCATTCATTATTAAC	Forward primer for generation of linearized pEVS143-*luxCDABE*
FJS-O025	TTAATTAACTCGAGCGGTACC	Reverse primer for generation of linearized pEVS143-*luxCDABE*
FJS-O407	catgcggcgggtaccgctcgagttaattaaGTGGTTTCTTATGAAGTCCATAC	Forward primer for the insertion of *luxC* promoter from *V. campbellii* into pEVS143-*luxCDABE* (5)
FJS-O408	gttaataatgaatgaaatttttttagtcatttcTTGCCCATTTATTATTAAAGGTAAG	Reverse primer for insertion of the *luxC* promoter from *V. campbellii* into pEVS143-*luxCDABE* (5)
FJS-O428	catgcggcgggtaccgctcgagttaattaaTAACGGCGTGAGGTACGAAC	Forward primer for insertion of the *qrr*1 promoter into pEVS143-*luxCDABE*
FJS-O429	gttaataatgaatgaaatttttttagtcat**ttcacacctcctgtac**CTAATATATCAGCATGCTTTATGCC	Reverse primer for insertion of the *qrr*1 promoter into pEVS143-*luxCDABE*
FJS-O430	catgcggcgggtaccgctcgagttaattaaAGTGGTTGCTTATGAATCAATC	Forward primer for insertion of the *qrr*2 promoter into pEVS143-*luxCDABE*
FJS-O431	gttaataatgaatgaaatttttttagtcat**ttcacacctcctgtac**AGAAGTATTATGCATTAATCATGCC	Reverse primer for insertion of the *qrr*2 promoter into pEVS143-*luxCDABE*
FJS-O432	catgcggcgggtaccgctcgagttaattaaCAGCCTTAGCAGGCTCGG	Forward primer for insertion of the *qrr*3 promoter into pEVS143-*luxCDABE*
FJS-O433	gttaataatgaatgaaatttttttagtcat**ttcacacctcctgtac**ATTTATATAATGCAGTTACTGTGCCAAC	Reverse primer for insertion of the *qrr*3 promoter into pEVS143-*luxCDABE*
RIMD *qrr*4 promoter	ggcgggtaccgctcgagttaattaaCTGAGGTATTTTTCCTCATTAATTAGCAGTATAGGGTAAAAATATGAAAGCTAATGGATAATCATAAAGTAGTAGTTGGTTTTTTGCTGAGAAAGTGATTAGTAGCAATGTAACAAGTGGCATATTTGCATGCTATTGCATTTTGCAAATGCAATTTGCGAAAGTGCTGGTTAATAATGCGTCGATATGCACCTGGATCTATTAAAAAACGGCTTTTTTAAAGTTGGCACGCATCGTGCTTTATCTAGAGGTACAGGAGGTGTGAA**gtacaggaggtgtgaa**atgactaaaaaaatttcattcatta	Synthetic fragment for insertion of the *qrr*4 promoter region into pEVS143-*luxCDABE*
FJS-O436	catgcggcgggtaccgctcgagttaattaaGCAGCTGACGTTTCTCGTG	Forward primer for insertion of the *qrr*5 promoter into pEVS143-*luxCDABE*
FJS-O437	gttaataatgaatgaaatttttttagtcat**ttcacacctcctgtac**ATAGTACTAAAGCATGAGGCG	Reverse primer for insertion of the *qrr*5 promoter into pEVS143-*luxCDABE*

FJS-O359	catgcggcgggtaccgctcgagttaattaaATTATTCACCTATAGTTGTTATAAATCC	Forward primer for insertion of the *cpsA* promoter into pEVS143-*luxCDABE*
FJS-O360	gttaataatgaatgaaatttttttagtcatGACCTAGTTTCCCTTCTAGC	Reverse primer for insertion of the *cpsA* promoter into pEVS143-*luxCDABE*
FJS-O250	catgcggcgggtaccgctcgagttaattaaAGCCATTTTATGAAACTTAACATATTG	Forward primer for insertion of the *scrA* promoter into pEVS143-*luxCDABE*
FJS-O251	gttaataatgaatgaaatttttttagtcatTTTTTTCGATCCTTGTCGG	Reverse primer for the insertion of the *scrA* promoter into pEVS143-*luxCDABE*
FJS-O063	gtaccgctcgagttaattaaTACTTTTCTCGTTTTAGATTTTC	Forward primer for insertion of the *lafA* promoter into pEVS143-*luxCDABE*
FJS-O064	gaatgaaatttttttagtcatCTTAGTCTCCTTAGTTTATCAC	Reverse primer for insertion of the *lafA* promoter into pEVS143-*luxCDABE*
FJS-S371	CGCAACCAGGATCCGGTG	Forward primer for generation of linearized pEVS143-*araC*-P_{bad}
FJS-S372	ATGGAGAAACAGTAGAGAGTTGC	Reverse primer for generation of linearized pEVS143-*araC*-P_{bad}
FJS-S375	ttttatcgcaactctctactgtttctccatTGCTTAAAGCAATTATTAAAATAATCAATTAG	Forward primer for insertion of the *opaR* 5'UTR region into pEVS143-*araC*-P_{bad} / pEVS143-*araC*-P_{bad}-*opaR-5'UTR-gfp*
FJS-S376	tttagacatggtaccAGTTCTAGGTCTCTTTGCAATTG	Reverse primer for insertion of the *opaR* 5'UTR region into pEVS143-*araC*-P_{bad} / pEVS143-*araC*-P_{bad}-*opaR-5'UTR-gfp*
FJS-S377	aagagacctagaactGGTACCATGTCTAAAGGTGAAG	Forward primer for insertion of the *gfpmut3* gene into pEVS143-*araC*-P_{bad} / pEVS143-*araC*-P_{bad}-*opaR-5'UTR-gfp*
FJS-S378	tgctcaatcaatcaccggatcctggttgcgTTATTTGTATAGTTCATCCATGCC	Reverse primer for insertion of the *gfpmut3* gene into pEVS143-*araC*-P_{bad} / pEVS143-*araC*-P_{bad}-*opaR-5'UTR-gfp*
FJS-q007	CCAAATGACAGCAGCGATAAG	Forward primer against the RIMD *ompW* gene
FJS-q008	GAACATGTAGCCAAACGTCAAA	Reverse primer against the RIMD *ompW* gene
FJS-q009	CTGCTGACTCTGATTGTGCTG	Forward primer against the φVP882 *gp69* gene

FJS-q010	TCGTGAGAGGTGATGTACTTCTC	Reverse primer against the φVP882 *gp69* gene
FJS-q001	TATGCGTGGCGGGTGAAA	Forward primer against the φVP882 *cos* site
FJS-q002	AGCCCAAACCGACGGAAA	Reverse primer against the φVP882 *cos* site
FJS-q053	CAACACCCAAGGCAATATACA	Forward primer against the φVP882 *IRS* site
FJS-q054	CACACCTAGCCCTATACCTATG	Reverse primer against the φVP882 *IRS* site

131 *FJS-O primers were used for cloning. FJS-q primers were used for quantitative PCR.

132 **All sequences are listed in the 5' to 3' direction. Lowercase letters represent overlaps for

133 homologous recombination. Underlined letters represent locations of point mutations. Bold letters

134 represent synthetic ribosome binding sites.

135

136 **S3 Table. Plasmids used in this study.**

Plasmid	Description	Identifier	Reference
pRE112	Sucrose counterselectable vector for allelic exchange ; Cm^r		(6)
pRE112-Δ*cpsA*	Allelic exchange vector for the clean deletion of *cpsA* (*VPA1403*) ; Cm^r	FJS-P025	This study
pRE112-Δ*pomA*	Allelic exchange vector for the clean deletion of *pomA* (*VP0689*) ; Cm^r	FJS-P008	This study
pRE112-$luxO^{D61E}$	Allelic exchange vector for the introduction of the $luxO^{D61E}$ point mutation (*VP2099*) ; Cm^r	FJS-P013	This study
pRE112-$luxO^{D61A}$	Allelic exchange vector for the introduction of the $luxO^{D61A}$ point mutation (*VP2099*) ; Cm^r	FJS-P014	This study
pRE112-Δ*opaR*	Allelic exchange vector for the clean deletion of *opaR* (*VP2516*) ; Cm^r	FJS-P015	This study
pRE112-Δ*scrABC*	Allelic exchange vector for the clean deletion of *scrABC* (*VPA1513-VPA1511*) ; Cm^r	FJS-P037	This study
φVP882::Cm^r	φVP882 with Tn5 inserted at a neutral locus. Tn5 includes Cm^r resistance cassette and an *oriT* site for conjugative transfer of the φVP882 genome	JSP-002	(4)
pEVS143-*araC*-P_{bad}-*vqmAφ*	Arabinose-inducible *vqmAφ* overexpression vector (P_{bad}-*vqmAφ*) ; Kan^r	pJES-052	(4)
pEVS143-*araC*-P_{bad}-*q*	Arabinose-inducible *q* overexpression vector (P_{bad}-*q*) ; Kan^r	pJES-093	(4)
pXB300	Tetracycline-inducible overexpression vector pXB300 ; Amp^r		(7)
pXBCm	Cm-resistant derivative of tetracycline-inducible overexpression vector pXB300 ; Cm^r	FJS-P061	This study
pXBCm-*qrr2*	Tetracycline-inducible *qrr2* overexpression vector (P_{tet}-*qrr2*) ; Cm^r	FJS-P063	This study
pXBCm-*opaR*	Tetracycline-inducible *opaR* overexpression vector (P_{tet}-*opaR*) ; Cm^r	FJS-P067	This study
pXBCm-*scrABC*	Tetracycline-inducible *scrABC* overexpression vector (P_{tet}-*scrABC*) ; Cm^r	FJS-P068	This study
pXBCm-$scrC^{E554A}$	Tetracycline-inducible $scrC^{E554A}$ (phosphodiesterase-null version of ScrC) overexpression vector (P_{tet}-$scrC^{E554A}$) ; Cm^r	FJS-P074	This study

pXBCm-*tpdA*	Tetracycline-inducible *tpdA* overexpression vector (P_{tet}-*tpdA*) ; Cm^r	FJS-P080	This study
pXBCm-*gefA*	Tetracycline-inducible *gefA* overexpression vector (P_{tet}- *gefA*) ; Cm^r	FJS-P081	This study
pEVS143-P_{luxC}-*luxCDABE*	Transcriptional reporter of the QS-regulated *luxC* promoter from *V. campbellii* strain BB120 fused to the *lux* operon ; Kan^r	FJS-P073	This study
pEVS143-P_{qrr1}-*luxCDABE*	Transcriptional reporter of the RIMD *qrr*1 sRNA promoter fused to the *lux* operon ; Kan^r	FJS-P075	This study
pEVS143-P_{qrr2}-*luxCDABE*	Transcriptional reporter of the RIMD *qrr*2 sRNA promoter fused to the *lux* operon ; Kan^r	FJS-P076	This study
pEVS143-P_{qrr3}-*luxCDABE*	Transcriptional reporter of the RIMD *qrr*3 sRNA promoter fused to the *lux* operon ; Kan^r	FJS-P077	This study
pEVS143-P_{qrr4}-*luxCDABE*	Transcriptional reporter of the RIMD *qrr*4 sRNA promoter fused to the *lux* operon ; Kan^r	FJS-P078	This study
pEVS143-P_{qrr5}-*luxCDABE*	Transcriptional reporter of the RIMD *qrr*5 sRNA promoter fused to the *lux* operon ; Kan^r	FJS-P079	This study
pEVS143-P_{cpsA}-*luxCDABE*	Transcriptional reporter of the RIMD *cpsA* promoter fused to the *lux* operon ; Kan^r	FJS-P072	This study
pEVS143-P_{scrA}-*luxCDABE*	Transcriptional reporter of the RIMD *scrA* promoter fused to the *lux* operon ; Kan^r	FJS-P059	This study
pEVS143-P_{lafA}-*luxCDABE*	Transcriptional reporter of the RIMD *lafA* promoter fused to the *lux* operon ; Kan^r	FJS-P018	This study
pEVS143-*araC*-P_{bad}-*opaR-5'UTR-gfp*	Translational reporter consisting of the *opaR* 5' UTR fused to the *gfp* gene ; Kan^r	FJS-P082	This study
c-di-GMP biosensor	pMMB67EH vector containing *turboRFP* under the control of three c-di-GMP riboswitches (Bc3-Bc5), constitutively expressed AmCyan for normalization, and the *hok/sok* region from pXB300 ; Gm^r	pFY4535	(8)

137

REFERENCES

1. Gode-Potratz CJ, McCarter LL. Quorum Sensing and Silencing in *Vibrio parahaemolyticus*. J Bacteriol. 2011;193(16):4224–37.

2. Makino K, Oshima K, Kurokawa K, Yokoyama K, Uda T, Tagomori K, et al. Genome sequence of *Vibrio parahaemolyticus*: a pathogenic mechanism distinct from that of *V cholerae*. The Lancet. 2003;361(9359):743–9.

3. Lan SF, Huang CH, Chang CH, Liao WC, Lin IH, Jian WN, et al. Characterization of a New Plasmid-Like Prophage in a Pandemic *Vibrio parahaemolyticus* O3:K6 Strain. Appl Environ Microbiol. 2009;75(9):2659–67.

4. Silpe JE, Bassler BL. A Host-Produced Quorum-Sensing Autoinducer Controls a Phage Lysis-Lysogeny Decision. Cell. 2019;176(1–2):268-280.e13.

5. Hustmyer CM, Simpson CA, Olney SG, Rusch DB, Bochman ML, Van Kessel JC. Promoter Boundaries for the *luxCDABE* and *betIBA-proXWV* Operons in *Vibrio harveyi* Defined by the Method Rapid Arbitrary PCR Insertion Libraries (RAIL). J Bacteriol. 2018;200(11):e00724-17.

6. Edwards RA, Keller LH, Schifferli DM. Improved allelic exchange vectors and their use to analyze 987P fimbria gene expression. Gene. 1998;207(2):149–57.

7. Bina XR, Wong EA, Bina TF, Bina JE. Construction of a tetracycline inducible expression vector and characterization of its use in *Vibrio cholerae*. Plasmid. 2014;76:87–94.

8. Zamorano-Sánchez D, Xian W, Lee CK, Salinas M, Thongsomboon W, Cegelski L, et al. Functional Specialization in *Vibrio cholerae* Diguanylate Cyclases: Distinct Modes of Motility Suppression and c-di-GMP Production. mBio. 2019;10(2):e00670-19.